iScience

CellPress
OPEN ACCESS

Article

SPARC regulation of PMN clearance protects from pristane-induced lupus and rheumatoid arthritis

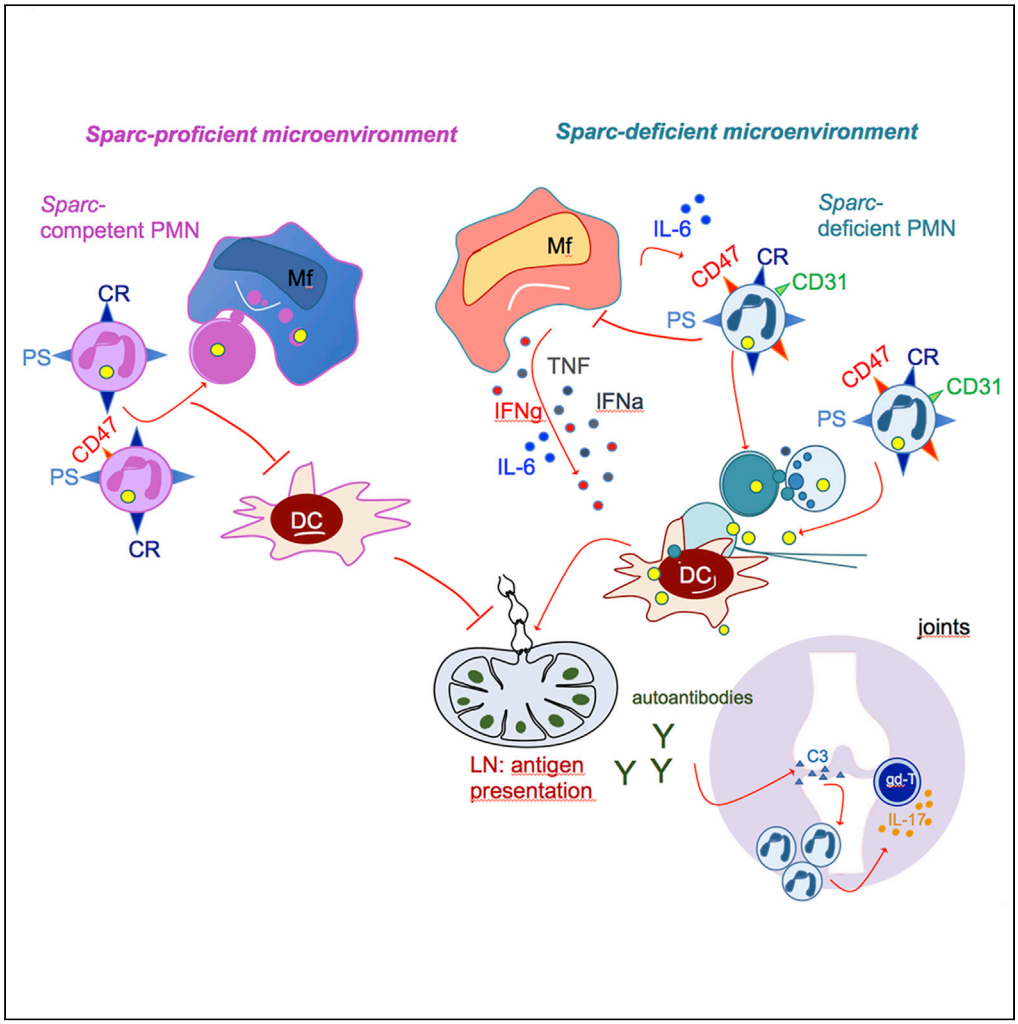

Sabina Sangaletti, Laura Botti, Alessandro Gulino, ..., Matteo Dugo, Claudio Tripodo, Mario P. Colombo

sabina.sangaletti@istitutotumori.mi.it (S.S.)
mariopaolo.colombo@istitutotumori.mi.it (M.P.C.)

Highlights

SPARC down-modulation is a necessary step toward autoimmunity and rheumatoid arthritis

SPARC controls neutrophil clearance regulating "don't-eat-me" signals and inflammation

Neutrophils escaping macrophage scavenging are source of antigens for dendritic cells

Sangaletti et al., iScience 24, 102510
June 25, 2021
https://doi.org/10.1016/j.isci.2021.102510

iScience

CellPress
OPEN ACCESS

Article

SPARC regulation of PMN clearance protects from pristane-induced lupus and rheumatoid arthritis

Sabina Sangaletti,[1,4,*] Laura Botti,[1] Alessandro Gulino,[2] Daniele Lecis,[1] Barbara Bassani,[1] Paola Portararo,[1] Matteo Milani,[1] Valeria Cancila,[2] Loris De Cecco,[3] Matteo Dugo,[3] Claudio Tripodo,[2] and Mario P. Colombo[1,*]

SUMMARY

The secreted protein acidic and rich in cysteine (SPARC) is a matricellular protein with unexpected immunosuppressive function in myeloid cells. We investigated the role of SPARC in autoimmunity using the pristane-induced model of lupus that, in mice, mimics human systemic lupus erythematosus (SLE). *Sparc*$^{-/-}$ mice developed earlier and more severe renal disease, multi-organ parenchymal damage, and arthritis than the wild-type counterpart. *Sparc*$^{+/-}$ heterozygous mice showed an intermediate phenotype suggesting *Sparc* gene dosage in autoimmune-related events. Mechanistically, reduced *Sparc* expression in neutrophils blocks their clearance by macrophages, through defective delivery of don't-eat-me signals. Dying *Sparc*$^{-/-}$ neutrophils that escape macrophage scavenging become source of autoantigens for dendritic cell presentation and are a direct stimulation for γδT cells. Gene profile analysis of knee synovial biopsies from SLE-associated arthritis showed an inverse correlation between SPARC and key autoimmune genes. These results point to SPARC down-regulation as a leading event characterizing SLE and rheumatoid arthritis pathogenesis.

INTRODUCTION

Autoimmunity results from multiple events dysregulating immune responses toward abnormal recognition of self-antigens, loss of tolerance, and the consequent attack of healthy cells and tissues.

The pathogenesis of autoimmune diseases combines genetic and epigenetic factors with environmental stressors, such as persistent inflammatory conditions, infections, and tissue damage (Costenbader and Karlson, 2006; Rosenblum et al., 2015).

Systemic lupus erythematosus (SLE) is a prototypical highly complex autoimmune disease characterized by circulating autoantibodies to nuclear and cytoplasmic antigens and by widespread involvement of the skin, joints, and parenchymal organs (Dorner and Furie, 2019). Although autoantibodies to DNA are a consistent finding in SLE, their direct role in determining the tissue/organ damage has been revised in favor of a more complex interaction between innate and adaptive autoimmunity (Bagavant and Fu, 2005). In systemic vasculitis (SV) clinical and experimental evidences support a pathogenesis driven by anti-neutrophil cytoplasmic autoantibodies (ANCAs). In SV, ANCAs induce neutrophil extracellular traps (NETs) (Heeringa et al., 2018) that, composed by extracellular DNA threads decorated with proteolytic and potentially injuring enzymes, directly promote endothelial damage (Kessenbrock et al., 2009). Moreover, the uptake by dendritic cells (DCs) of NET coated with antigens recognized by ANCA-Abs (antibodies), such as myeloperoxidase (MPO) and proteinase-3, begins and perpetuates the autoimmune responses by promoting ANCA induction (Sangaletti et al., 2012). In SLE, NETs are potent stimulators of pathogenic DCs (Garcia-Romo et al., 2011; Lande et al., 2011) and direct activators of human autoreactive memory B cells (Gestermann et al., 2018). Therefore any unbalance in NET formation can be linked with the pathogenesis of SLE and SV. In SLE, neutrophils are characterized not only by exacerbated NETosis but also by defective phagocytosis and microbial killing capacity, by increased oxidative stress and cytokine production; and by enhanced apoptosis (Tsai et al., 2019) (Kaplan, 2011). These defects are magnified by other phagocytic cell impairment, including defective macrophages efferocytosis. Indeed, patients with SLE often display a deficiency in clearing apoptotic cells and immune complexes (ICs) (Munoz et al. [2010], Baumann et al., [2002]; Davies et al. [2002]) and also defective expression of monocytes adhesion molecules like CD44 (Cairns et al., 2001).

[1]Molecular Immunology Unit, Department of Research, Fondazione IRCCS Istituto Nazionale dei Tumori di Milano, Milan, Italy

[2]Tumor Immunology Unit, University of Palermo, Palermo, Italy

[3]Platform of Integrated Biology, Department of Applied Research and Technology Development, Fondazione IRCCS Istituto Nazionale dei Tumori di Milano, Milan, Italy

[4]Lead contact

*Correspondence: sabina.sangaletti@istitutotumori.mi.it (S.S.), mariopaolo.colombo@istitutotumori.mi.it (M.P.C.)

https://doi.org/10.1016/j.isci.2021.102510

The secreted protein acidic and rich in cysteine (SPARC) is a multi-faced matricellular protein involved in normal and pathological tissue remodeling (Puolakkainen et al., 2003; Trombetta-Esilva and Bradshaw, 2012) and capable of affecting, either positively or negatively, cell-cell and cell-ECM adhesive interactions (Brekken and Sage, 2001). SPARC binds to different collagens and directly regulates their assembly. The most evident phenotype of *sparc* deficiency is the lens opacity that develops in mice beginning at 1.5 months of age, the lens capsule being composed of more than 90% of type IV collagen (Norose et al., 1998). The capacity of SPARC to interfere with fibers deposition also affects tissue fibrosis; indeed Sparc−/− mice are protected from the development of lung and bone marrow (BM) fibrosis, modeled by bleomycin and rTPO injection, respectively (Sangaletti et al., 2011; Tripodo et al., 2012). Sparc-deficient mice are also characterized by osteopenia, as sparc is critical in the support of bone remodeling and maintenance of bone mass (Delany et al., 2000).

An underinvestigated but interesting aspect of SPARC function is related to its capacity of regulating the immune system functions in several aspects such as DC migration and branching (Piconese et al., 2011), myeloid-derived suppressor cell expansion and functional differentiation (Sangaletti et al., 2019), and, more in general, inflammation. *Sparc*$^{-/-}$ mice are characterized by exacerbated inflammatory responses. On the one hand, Sparc deficiency protects from the development of lung fibrosis, and on the other hand, the same treatment induces a strong inflammatory condition close to pulmonitis under the same bleomycin treatment. Mechanisms through which SPARC exerts anti-inflammatory responses include a negative regulation of transforming growth factor-β and nuclear factor (NF)-κB signaling (Sangaletti et al., 2011, 2019). Other than immune cell functions SPARC may also have an impact on immune cell development, for example, B cell development (Luo et al., 2014; Sangaletti et al., 2014a). Studying mesenchymal cell functions in BM and secondary lymphoid organs we showed that the defective B cells development occurring in *Sparc*$^{-/-}$ hosts under radiation-induced stress relies on SPARC limiting B cell precursors' apoptosis (Sangaletti et al., 2014a). Furthermore, in *Fas* mutant mice we showed that neutrophils from *Sparc*$^{-/-}$ mice were more supportive for B cell transformation through an increased expression of BAFF and interleukin (IL)-21 and increased NETosis (Sangaletti et al., 2014b). These evidences suggested an involvement of SPARC in the regulation of immune cell death, a key immunological checkpoint to prevent autoimmunity.

To investigate the functional role of SPARC in SLE, we adopted a chemically induced model of autoimmunity, namely, intraperitoneal (i.p.) injection of the hydrocarbon oil 2,6,10,14-tetramethylpentadecane (TMPD), more commonly known as pristane, which induces a systemic lupus-like disease in BALB/c mice. This model recapitulates several major clinical manifestations of human lupus including glomerulonephritis, lung vasculitis and arthritis, accumulation of autoantibodies to single-stranded (ss) and double-stranded (ds) DNA and to ribonucleoproteins (RNP), as well as the female sex-biased incidence of the disease and the dependency on interferon (IFN) for disease initiation (Reeves et al., 2009).

RESULTS

SPARC protects mice from onset of SLE-like disease

Mice treated with pristane develop an SLE-like disease characterized by multiorgan damage and autoantibodies (Reeves et al., 2009). We injected pristane i.p. in wild-type (WT) and *Sparc*$^{-/-}$ mice that were monitored over a 300-day period. Histopathological analysis of the kidney revealed that differently from WT mice, which displayed glomerular atrophy, *Sparc*$^{-/-}$ mice developed earlier and more severe renal disease with glomerular hypercellularity, sclerosis with the presence of immune infiltrates, lipoid tubular degeneration, and also glomerular necrosis (Figure 1A, right, inset). *Sparc*$^{-/-}$ mice also showed more severe lung injury on histopathology, with signs of alveolar hemorrhage and massive hemosiderin-laden histiocytic infiltration (Figure 1B). In addition to kidney and lung damage, the liver of *Sparc*$^{-/-}$ mice showed more severe signs of portitis evolving to steatohepatitis than WT liver counterpart (Figure 1C). However, the most prominent phenotype due to SPARC deficiency was detected in the joints. Indeed, *Sparc*$^{-/-}$ mice had increased and anticipated occurrence of arthritis (130 days versus 220 days) (Figures 1D and 1E) in one or more paws and more severe manifestations of arthritis than the *Sparc*-proficient counterpart (Figure 1F). Histological examination of arthritic damage at 130 and 220 days post-pristane injection showed that paws from *Sparc*$^{-/-}$ mice were heavily infiltrated by a mixed population of immune cells mostly composed by polymorphonuclear granulocytes and, to a lesser extent, lymphocytes (Figure 1G).

Consistent with the more severe phenotype occurring in *Sparc*$^{-/-}$ mice, their sera, evaluated 130 days post-pristane, were characterized by the enrichment in autoantibodies against self-nuclear antigens (Figure 1H),

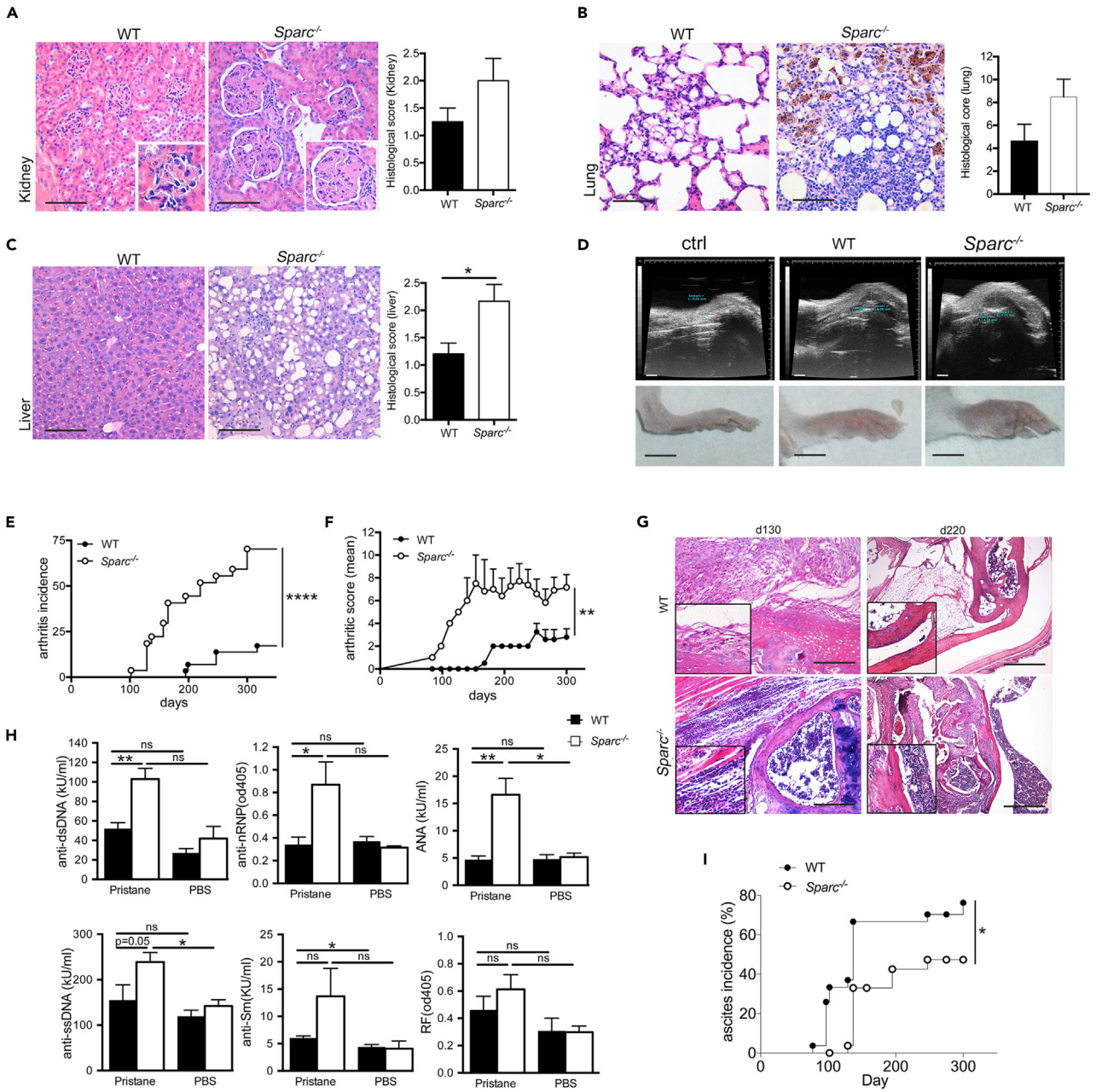

Figure 1. SPARC deficiency causes accelerated production of autoantibody and exacerbated organ damage

(A) Representative histology of kidneys from WT and *Sparc*$^{-/-}$ mice 300 days after initiation of the experiment showing more severe organ damage of the latter group of animals (left) and histological score evaluated on 5 mice per group (right); inset, a glomerulus at higher magnification. Scale bars, 100 μm.

(B) Representative histology (left) and histological score (right) of lung from the indicated mice.

(C) As in (A), representative image and score of liver (*$p < 0.05$ Mann-Whitney test, mean ± SEM); scale bars, 100 μm.

(D) The upper panel shows a representative ultrasound (US) echographic examination of the arthritic paw of pristane-treated WT and *Sparc*$^{-/-}$ mice (scale bars, 1 mm). The lower panel shows representative pictures of paws from WT and *Sparc*$^{-/-}$ at day 200 after pristane injection; scale bars, 0.5 cm.

(E–H) Kinetic analysis of arthritis incidence; (WT n = 15; *Sparc*$^{-/-}$ n = 20; pooled from two independent experiments; ****$p < 0.0001$, log-rank [Mantel-Cox] test). (F) Arthritis score obtained evaluating pristane-treated mice every 2 weeks (WT n = 15; *Sparc*$^{-/-}$ n = 20; pooled from two independent experiments; **$p < 0.01$, multiple t test, Bonferroni-Dunn method [mean ± SEM]). (G) Representative H&E staining of arthritic paws at days 130 and 220 after pristane injection. (H) Total serum Igs against the indicated self-antigens have been dosed in untreated mice or mice 130 days after pristane treatment (n = 7 for treated mice and n = 4 for untreated controls; *$p < 0.05$; **$p < 0.01$, one-way ANOVA, Tukey adjusted multiple comparison; mean ± SEM). One experiment representative out of three is shown.

(I) Ascites development in WT and *Sparc*$^{-/-}$ mice (WT n = 15; *Sparc*$^{-/-}$ n = 20; pooled from two independent experiments; *$p < 0.05$, long-rank [Mantel-Cox] test).

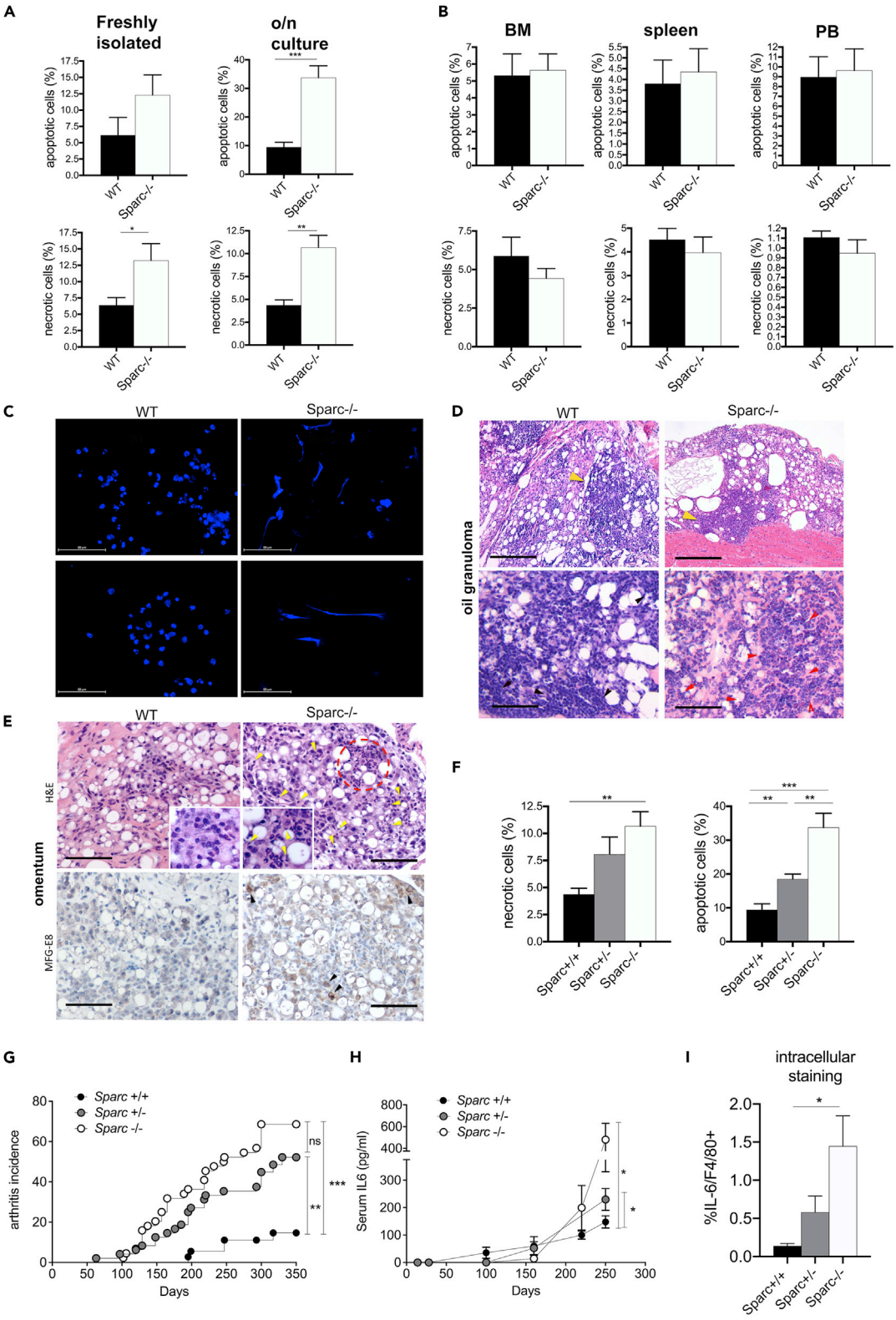
A
Freshly isolated
o/n culture
apoptotic cells (%)
necrotic cells (%)
WT
Sparc-/-
B
BM
spleen
PB
C
D
oil granuloma
E
omentum
H&E
MFG-E8
F
Sparc+/+
Sparc+/-
Sparc-/-
G
arthritis incidence
Sparc +/+
Sparc +/-
Sparc -/-
Days
ns
H
Serum IL6 (pg/ml)
I
intracellular staining
%IL-6/F4/80+

Figure 2. Accumulation of dying PMN in pristane-treated Sparc$^{-/-}$ mice

(A–I) (A) Frequency of apoptosis (Annexin V^{+}7AAD^{+}) and necrosis (Annexin V^{-}7AAD^{+}) in PMN isolated from the peritoneal wash of pristane-treated WT and *Sparc*$^{-/-}$ mice (day 130) showing a preferential accumulation of necrotic and apoptotic PMN in *Sparc*$^{-/-}$ mice; the same analysis, performed on the same cells cultured o/n, shows an amplification of the trend observed in freshly isolated PMN (*p < 0.05; **p < 0.01; ***p < 0.001, Unpaired *t* test, Mean ± SEM). (B) The frequency of apoptotic and necrotic PMN isolated from the BM, spleen, and peripheral blood from the same mice showing no changes among the two groups (n = 7/group, representative of 5 experiments). (C) NET formation by peritoneal PMN isolated from WT and *Sparc*$^{-/-}$ mice (day 130 after pristane treatment). PMN were seeded onto poly-D-lysine-coated glasses without any additional stimuli (DAPI staining). Scale bars, 50 μm. (D) H&E staining of OG sections of the indicated mice at day 200 post-pristane treatment showing enrichment of PMN in OG from SPARC-deficient mice (scale bars: 500 μm in upper panel and 100 μm in lower panel). (E) H&E staining (upper panels; scale bars, 100 μm) and MFG-E8 (lower panels; scale bars, 100 μm) of omentum sections showing the predominance of lymphoid cells in WT mice conversely to the enrichment in PMN foci in *Sparc*$^{-/-}$ mice (red dotted circle). Omentum from *Sparc*$^{-/-}$ mice also shows a massive presence of cellular debris (yellow arrowheads) despite the presence in the same areas of macrophages producing MFG-E8 (lower panel, back arrowheads). (F) Frequency of apoptosis (Annexin V^{+}7AAD^{+}) and necrosis (Annexin V^{-}7AAD^{+}) in PMN isolated from the peritoneal wash of pristane-treated heterozygous *Sparc*$^{+/-}$ mice compared with WT and *Sparc*$^{-/-}$ counterparts (day 130). **p < 0.01; ***p < 0.001; one-way ANOVA, Tukey adjusted multiple comparison test. Mean ± SEM is shown. (G) Kinetic analysis of arthritis incidence in heterozygous *Sparc*$^{+/-}$ mice compared with WT (*Sparc*$^{+/+}$) and *Sparc*$^{-/-}$ mice (**p < 0.01; ***p < 0.001 log-rank [Mantel-Cox] test). (H) Serum IL-6 level in pristane-treated mice (pg/mL); (n = 6/group) (day 110); mean ± SEM is shown; *p < 0.05; one-way ANOVA, Tukey adjusted multiple comparison test. (I) Frequency of F4/80+ cells expressing IL-6 in peritoneal wash from pristane-treated WT, Sparc$^{-/-}$, and Sparc$^{+/-}$ mice (n = 8/group) (intracellular staining FACS analysis, day 110, mean ± SEM; *p < 0.05; one-way ANOVA, Tukey adjusted multiple comparison test).

including dsDNA, nRNP, antinuclear antibodies. Notably, at the same time point, the *Sparc*-proficient WT counterpart did not show any significant production of autoantibodies. The difference was equalized at later time points, the level of autoantibodies being very similar 200 days post-pristane treatment (not shown). This suggests an anticipated onset of autoantibody production in *Sparc*–/– mice. Of note, the onset of this phenotype was independent of the development of ascites that was reduced in *Sparc*–/– rather than in WT mice (Figure 1I). Overall, these data suggest that SPARC down-modulation might take part in the mechanisms leading to the development of SLE and rheumatoid arthritis (RA) in pristane-treated mice. In line, gene expression profile (GEP) analysis of mesenteric lymph nodes (LNs) and spleens from BALB/c and DBA-2 mice (Database: GSE17297; [Zhang et al., 2009]) showed that *Sparc* was expressed only in secondary lymphoid organs from the susceptible BALB/c strain and that it was down-regulated upon pristane injection, starting 4 days after treatment (Figure S1).

Pristane-elicited PMN undergo accelerated cell death in *Sparc*$^{-/-}$ mice

We reasoned that one key event that might explain the earlier autoantibody production occurring in *Sparc*–/– mice could be ascribed to an increased and early availability of autoantigens. The injection of pristane in mice leads to a persistent inflammatory response in the peritoneal cavity, with massive recruitment of polymorphonuclear leukocytes (PMN) that represent, upon death, a potentially relevant source of immunogenic cytoplasmic and nuclear self-antigens. Indeed, any abnormality in their clearance is potentially able to increase the availability of otherwise undetectable immunogenic autoantigens through the induction of secondary necrosis or NETosis.

Annexin V/7-AAD profile examination of cells freshly isolated from the peritoneal cavity showed increased frequency of necrotic and apoptotic cells in pristane-treated *Sparc*$^{-/-}$ mice than WT counterpart (Figure 2A). This difference became significant after culturing PMN overnight (o/n) (Figure 2A). Notably, the difference was restricted to the peritoneal cavity (the site of inflammation) and did not involve other organs, neutrophil apoptosis and necrosis being similar between Sparc-deficient and -proficient mice when evaluated in BM, spleen, and peripheral blood leukocytes (Figure 2B). We then evaluated the capacity of *Sparc*$^{-/-}$ and WT PMN to undergo NETosis. In agreement with our previous study performed in MRL-Lpr either crossed or not with *Sparc*$^{-/-}$ mice (Sangaletti et al., 2014b), the PMN isolated from the peritoneal cavity of pristane-treated *Sparc*$^{-/-}$ mice showed increased spontaneous capacity to extrude NET than similarly treated WT counterpart (Figure 2C).

In addition, abundant autoantigens can be found in tertiary ectopic lymphoid structures in the form of oil granulomas (OGs) that develop in the peritoneal cavity of pristane-treated mice and that represent the primary sites of autoreactive B cells activation in this model. Also, OG (Figure 2D) and omentum (Figure 2E) were mainly populated by lymphoid cells or PMN in WT and *Sparc*$^{-/-}$ mice, respectively. In the omentum of Sparc$^{-/-}$ mice we identified consistent numbers of cellular debris (Figure 2E, upper panels, arrowheads) and apoptotic cells and the accumulation of macrophages competent for phagocytosis (MFG-E8 staining in Figure 2E, lower panels).

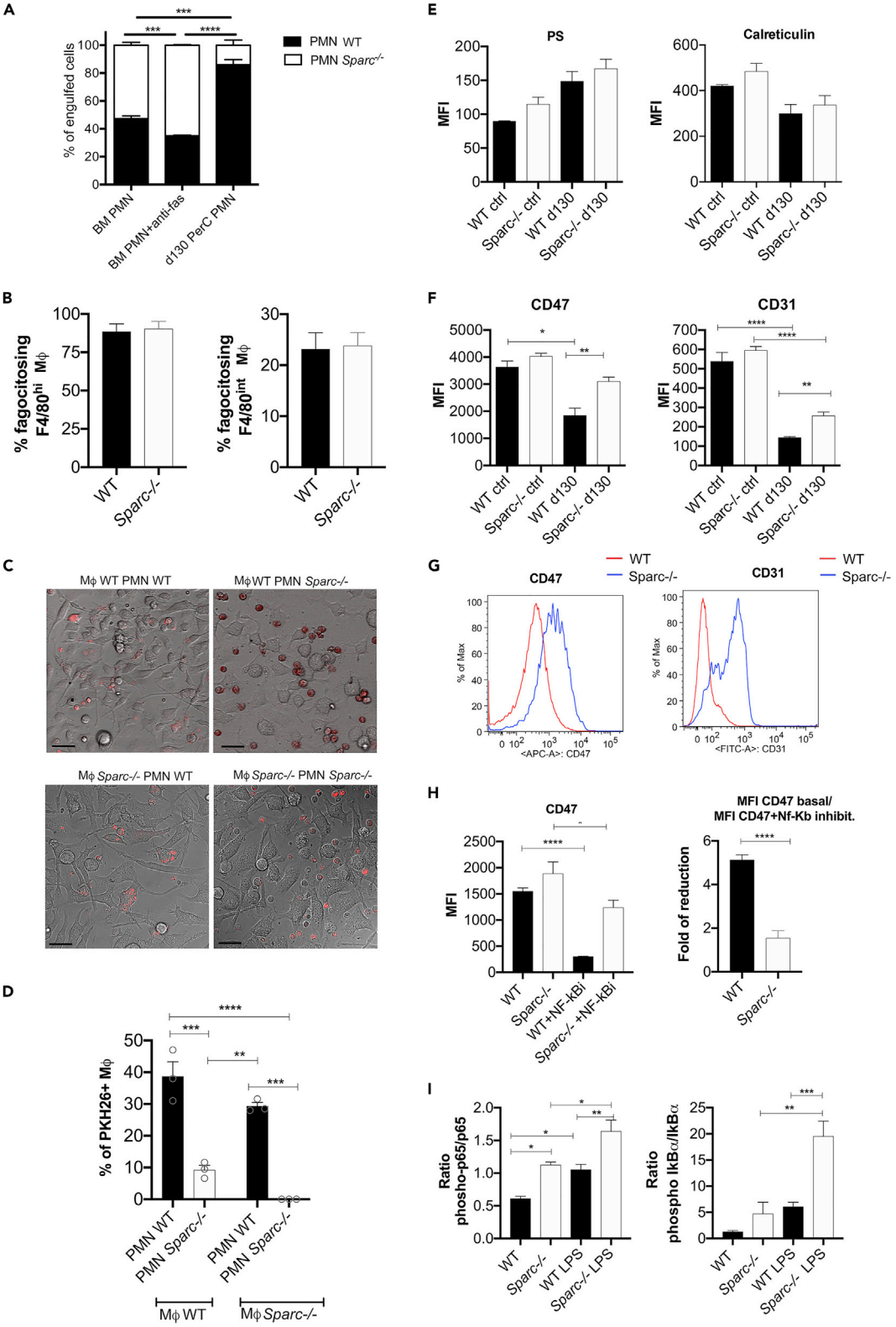
A
% of engulfed cells
PMN WT
PMN Sparc-/-
BM PMN
BM PMN+anti-fas
d130 PerC PMN
B
% fagocitosing F4/80hi Mϕ
% fagocitosing F4/80int Mϕ
WT
Sparc-/-
C
Mϕ WT PMN WT
MϕWT PMN Sparc-/-
Mϕ Sparc-/- PMN WT
Mϕ Sparc-/- PMN Sparc-/-
D
% of PKH26+ Mϕ
PMN WT
PMN Sparc-/-
Mϕ WT
Mϕ Sparc-/-
E
PS
Calreticulin
MFI
WT ctrl
Sparc-/- ctrl
WT d130
Sparc-/- d130
F
CD47
CD31
MFI
G
WT
Sparc-/-
CD47
CD31
% of Max
<APC-A>: CD47
<FITC-A>: CD31
H
CD47
MFI
MFI CD47 basal/
MFI CD47+Nf-Kb inhibit.
Fold of reduction
WT
Sparc-/-
WT+NF-kBi
Sparc-/- +NF-kBi
I
Ratio phosho-p65/p65
Ratio phospho IkBα/IkBα
WT
Sparc-/-
WT LPS
Sparc-/- LPS

Figure 3. SPARC deficiency associates to a defective clearance by macrophages of dying PMN

(A–I) (A) *In vitro* efferocytosis assay using WT peritoneal macrophages cultured 30 min with 1:1 ratio of WT and *Sparc*$^{-/-}$ peritoneal PMN or BM PMN (treated or not with anti-Fas Ab, to induce apoptosis, as control) (statistic: *** $p < 0.001$; ****$p < 0.0001$, Student's t test, mean ± SEM). The analysis highlights a specific defect in the clearance of *Sparc*$^{-/-}$ PerC PMN. (B) Percentage of F4/80hi and F4/80int peritoneal macrophages (Mφ) engulfing CFSE-labeled apoptotic Jurkat cells. (C) Time-lapse confocal microscopy and relative quantification of WT and *Sparc*$^{-/-}$ macrophages (unstained, bright field) co-cultured with either WT or *Sparc*$^{-/-}$ macrophages (Mφ, labeled with PKH26). Contrary to WT PMN that died and were almost completely engulfed by macrophages from both strains, *Sparc*$^{-/-}$ PMN accumulated in the co-culture without removal; scale bars, 10 μm. (D) Relative quantification; statistical analysis: one-way ANOVA, multiple comparisons test (Tukey). Mean ± SEM is shown; **$p < 0.01$; ***$p < 0.01$; ****$p < 0.0001$. (E) Expression of the "eat-me" (phosphatidylserine, PS, and calreticulin) and of (F) "don't-eat-me" (CD47 and CD31) signals in peritoneal WT and *Sparc*$^{-/-}$ PMN at day 130 after pristane treatment; statistical analysis: one-way ANOVA, multiple comparison test (Tukey). *$p < 0.05$; **$p < 0.01$; ****$p < 0.0001$; error bars indicate mean ± SEM. (G) Representative histogram plots showing the increased expression of CD47 and CD31 on *Sparc*$^{-/-}$ PMN compared with the WT counterpart (pristane treated day 130). (H) Mean fluorescence intensity (MFI) of expression of CD47 and the relative fold reduction in PMN isolated at day 130 after pristane treatment and following o/n treatment with the NF-κB activation inhibitor InSolution (n = 6/group). Statistical analysis: CD47 MFI, one-way ANOVA, multiple comparison test; fold of reduction: Student's t test (*$p < 0.05$, ****$p < 0.0001$). Error bars are mean ± SEM. (I) Phosphorylation of p65 and of Ikba in WT and *Sparc*−/− PMN treated for 2 h with LPS (n = 6/group). Data are expressed as ratio between phospho-p65/p65 and phospho IkBα/IkBα. Statistical analysis: one-way ANOVA, multiple comparison test *$p < 0.05$; **$p < 0.01$; ***$p < 0.001$ (Tukey). Error bars are mean ± SEM.

Overall these evidences suggest that the prevalent immunogenic cell death of *Sparc*−/− PMN and their specific enrichment in ectopic lymphoid structures are supportive for increased availability of autoantigen and their presentation in *Sparc*$^{-/-}$ mice. Corroborating this hypothesis, OG from pristane-treated *Sparc*$^{-/-}$ mice showed a higher incidence of pseudo-follicular structures that are suggestive of follicular B cell responses.

Susceptibility to PMN death is a known hallmark of SLE, and because our data indicate that SPARC deficiency predisposes to neutrophil death and SLE development, we analyzed PMN from peritoneal wash of pristane-treated heterozygous *Sparc*$^{+/-}$ mice and found intermediate level in the percentages of apoptotic and necrotic cells, between WT and *Sparc*$^{-/-}$ mice (Figure 2F). Notably, heterozygous *Sparc*$^{+/-}$ mice also showed intermediate arthritis incidence (Figure 2G) and of IL-6 serum (Figure 2H). The cellular source of IL-6 was identified as F4/80+ macrophages, as detected by intra-cellular staining and fluorescence-associated cell sorting (FACS) analysis (Figure 2I).

Reduced clearance of dying PMN in *Sparc*$^{-/-}$ mice is associated with defective modulation of "don't-eat-me" signals

Considering that markers of PMN activation such as CD62L and reactive oxygen species were equal in *Sparc*$^{-/-}$ and WT PMN upon PMA stimulation (not shown), we tested whether the increased accumulation of dying PMN in *Sparc*$^{-/-}$ mice depends on their defective or incomplete removal by phagocytes. WT and *Sparc*$^{-/-}$ thioglycollate-elicited macrophages were cultured 20 min with PMN isolated *ex vivo* from the peritoneal cavity of WT or *Sparc*$^{-/-}$ mice, 130 days after pristane treatment. To make a direct comparison, PMN were stained with distinct vital dyes (carboxyfluorescein succinimidyl ester [CFSE] for WT PMN and Cell Proliferation Dye eFluor 670 for *Sparc*$^{-/-}$ PMN) and mixed at 1:1 ratio before co-culture with macrophages. PMN from pristane-treated *Sparc*$^{-/-}$ mice were less efficiently phagocytosed than the WT counterparts (Figure 3A). To gain a rough information on the phagocytic activity of *Sparc*-proficient and -deficient macrophage, *in vivo* phagocytosis assay was performed by i.p. injection of UV-irradiated and CFSE-labeled apoptotic Jurkat cells into thioglycollate-treated Sparc-deficient or -sufficient mice: results showed that both resident large peritoneal macrophages and F4/80int monocyte-derived migratory macrophages (Ghosn et al., 2010) similarly engulfed apoptotic cells, regardless the *Sparc* genotype (Figure 3B). Overall, these data suggest that SPARC deficiency, per se, does not affect macrophage efferocytosis but rather that the clearance of *Sparc*$^{-/-}$ PMN is selectively defective. To confirm this possibility, we performed o/n time-lapse confocal microscopy analysis of PMN and macrophage co-cultures, documenting along time the interaction between macrophages and PMN as well as PMN cell death and their removal by macrophages. Specifically, WT and *Sparc*$^{-/-}$ PMN were labeled with the vital dye PKH26 and cultured with WT or *Sparc*$^{-/-}$ macrophages in all possible combinations (Figures 3C and 3D). Differently from WT PMN that were almost completely engulfed by macrophages regardless the *Sparc* macrophages genotype, *Sparc*$^{-/-}$ PMN persisted in the co-culture.

Time-lapse analysis clearly showed that the addition of *Sparc*$^{-/-}$ PMN to WT macrophages was sufficient to block macrophage movement, impeding contact with PMN. On the contrary, macrophages move rapidly, chase, and engulf WT PMN (Videos S1 and S2). These results suggested a defect in *Sparc*$^{-/-}$ PMN recognition. On this hypothesis, we evaluated the expression of "eat-me" (calreticulin and phosphatidylserine) and

"don't-eat-me" (CD47, CD31) signals (Bratton and Henson, 2011; Hart et al., 2000; Ravichandran, 2011) on PMN isolated from the peritoneal cavity of WT and *Sparc*$^{-/-}$ pristane-treated mice (day 130). *Sparc*$^{-/-}$ and WT PMN undergoing cell death showed similar expression of calreticulin and phosphatidylserine "eat-me" signals (Figure 3E); however, this expression in *Sparc*$^{-/-}$ mice was not paralleled by a corresponding down-regulation of "don't-eat-me" signals, particularly of CD47. Indeed, the expression of CD47 was retained and even up-regulated in *Sparc*$^{-/-}$ PMN when compared with WT PMN (Figure 3F-G). Analyzing CD31, another don't-eat-me signal, we found a similar trend with *Sparc*$^{-/-}$ PMN retaining CD31 expression higher than the WT counterpart (Figure 3F-G). This finding indicated a defective delivery of "eat-me" and "don't-eat-me" signals, in *Sparc*$^{-/-}$ PMN, associated with their impaired clearance. IL-6, which was higher in the serum of *Sparc*$^{-/-}$ than WT mice, might explain the sustained expression of CD47 and CD31 on *Sparc*$^{-/-}$ PMN because of unrestrained NF-κB activation. Supporting this possibility, different articles have recently shown NF-κB-induced CD47 up-regulation (Betancur et al., 2017). To directly test this point, PMN from pristane-treated WT and *Sparc*$^{-/-}$ mice (day 130) were cultured o/n in the presence of a cell-permeable NF-κB activation inhibitor and evaluated for CD47 expression. Results showed that NF-κB inhibitor reduced the expression of CD47 in WT but not in *Sparc*$^{-/-}$ PMN (Figure 3H). This suggests an intrinsic inability of *Sparc*$^{-/-}$ PMN of negatively regulating NF-κB signaling pathway. To challenge this hypothesis we performed a canonical assay in which PMN from WT and *Sparc*$^{-/-}$ mice were stimulated with lipopolysaccharide (LPS) for 2 h and evaluated for p65 and Ikba phosphorylation, by FACS analysis. We found strongly increased phospho-p65/p65 and phospho-IkBα/IkBα ratio (Figure 3I) in *Sparc*$^{-/-}$ than WT PMN. On the same line, *in vivo* inhibition of IL-6 by a monoclonal antibody (mAb) to its alpha chain receptor reduced CD47 and CD31 expression in WT but not *Sparc*$^{-/-}$ PMN collected from pristane-elicited mice (Figure S2).

Dying PMN that escape macrophage scavenging are source of autoantigens for DC presentation

Having shown that, in *Sparc*$^{-/-}$ mice, the defective clearance of dying PMN provides a great source of autoantigens, we explored whether *Sparc*$^{-/-}$ macrophages, although competent for the phagocytic activity, could contribute in worsening the autoimmune phenotype in *Sparc−/−* mice, supporting inflammatory pathways or antigen-presenting cell (APC) functions. As first approach, we compared the GEP of macrophages isolated from the peritoneal cavity of pristane-treated WT and *Sparc*$^{-/-}$ mice. Thirteen genes were up-regulated and 8 were down-regulated in *Sparc*$^{-/-}$ macrophages (Figure 4A and Table S1). Gene set enrichment analysis revealed up-regulation of gene sets proper of an inflammatory status, including TNF, IFNγ, and IFNα (Figure 4B, Table S2). Furthermore, metabolic pathways relevant for macrophages activity, such as cholesterol homeostasis (relevant for M1) and oxidative phosphorylation (relevant for M2), were up- or down-modulated, respectively, in *Sparc*$^{-/-}$ macrophages. These data support a preferential polarization toward an M1 phenotype (Diskin and Palsson-McDermott, 2018). In line, the GEP analysis shows that *Sparc*-deficient macrophages express significantly less Mrc1/CD206 than WT macrophages (FC = −2,023; $p < 0.05$, Table S1). These data are in line with the intracellular staining and FACS analysis of Figure 2H showing F4/80+ macrophages as the relevant source of IL-6 in pristane-treated and particularly in *Sparc*$^{-/-}$ mice.

This M1-deflected pro-inflammatory microenvironment suggested to investigate the antigen presenting functions of macrophages and DCs from *Sparc*$^{-/-}$ mice. The frequency of F4/80+ macrophages in draining LN was similar in both *Sparc*-proficient and -deficient mice (Figure 4C); however, a significantly higher frequency of DCs (CD11c^{hi}) was detected in *Sparc*$^{-/-}$ LN (Figure 4D), supporting the involvement of DCs in antigen presentation and T cells activation. In line, draining LN of pristane-treated *Sparc*$^{-/-}$ animals showed an increased frequency of activated CD4^{+} T cells skewed toward a central memory T cell phenotype (Figures 4E and 4F). Although not statistically significant, a trend toward increased IL-4 production by total CD4+ T cells was also observed (Figure 4G). This particular evidence finds correlation with patients with SLE (Banchereau and Pascual, 2006) and is in line with the increased titer of T cell-dependent Abs to dsDNA (Rekvig and Nossent, 2003) observed in *Sparc*$^{-/-}$ mice.

Overall, these results suggest that defective clearance of *Sparc*$^{-/-}$ PMN by macrophages could increase the fraction of autoantigens available for presentation by DCs. To gain more insight into this point, we modeled the cross-talk of dying PMN with macrophages and DCs, *in vitro*; o/n time-lapse confocal microscopy was set up co-culturing combinations of BM-derived macrophages and BM-derived DCs together with PMN isolated from the peritoneal cavity of pristane-treated mice. When PMN, macrophages, and DCs were from WT mice, we observed that PMN progressively underwent apoptosis and were readily

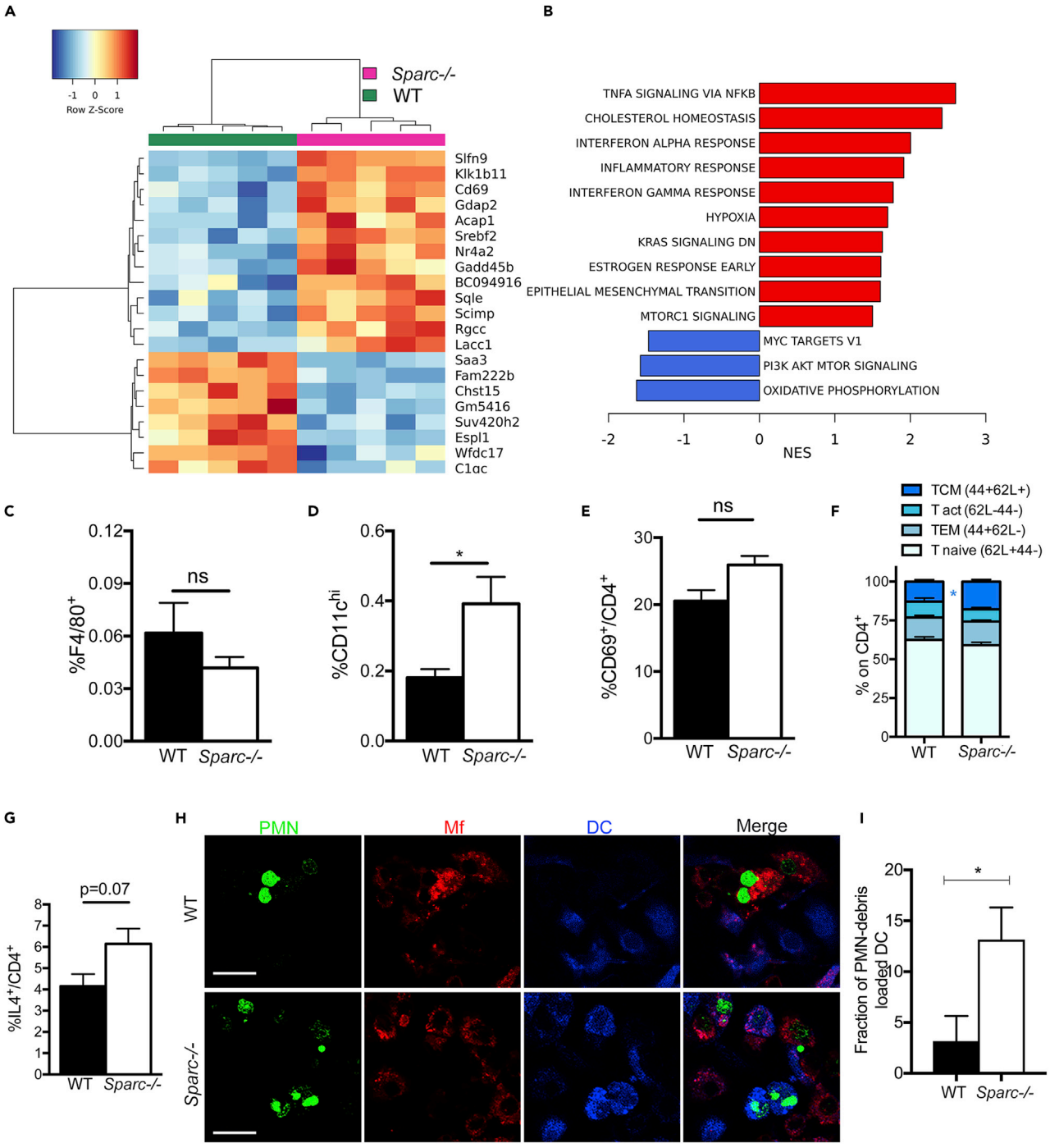

Figure 4. Increased DC activation and presentation in Sparc$^{-/-}$ mice

(A–I) (A) Heatmap of macrophages isolated from the peritoneal cavity of pristane-treated WT when compared with *Sparc*$^{-/-}$ mice. (B) Gene set enrichment analysis of WT and *Sparc*$^{-/-}$ macrophages. (C) Frequency of F4/80+ macrophages and (D) of dendritic cells (CD11c^{hi}) in mediastinal LN of pristane-treated WT and *Sparc*$^{-/-}$ mice (*p < 0.05, Student's t test; error bars are mean ± SEM). (E) Frequency of activated CD4^{+} T cells expressing CD69^{+} in draining mediastinal LN of pristane-treated WT and *Sparc*$^{-/-}$ mice (error bars are mean ± SEM). (F) Frequency of central memory (TCM CD44 + CD62L+), activated (T act CD44-CD62L-), effector memory (TEM CD44 + CD62L-), and naive CD4+ (CD44-CD62L+) cells in WT and *Sparc*−/− mice. Error bars are mean ± SEM. *p< 0.05, Student's t test. (G) Frequency of IL4+ CD4 T cells; (Student's t test; error bars are mean ± SEM). (H) Representative confocal microscopic analysis showing the preferential uptake of PMN debris (green) by DCs (blue) but not macrophages (red) in the *Sparc*$^{-/-}$ setting. Scale bar, 10 μm. (I) Cumulative data obtained by analyzing 5 samples/group for a total of n = 50 DCs and n = 50 macrophages. (Student's t test: *p < 0.05, error bars are mean ± SEM.)

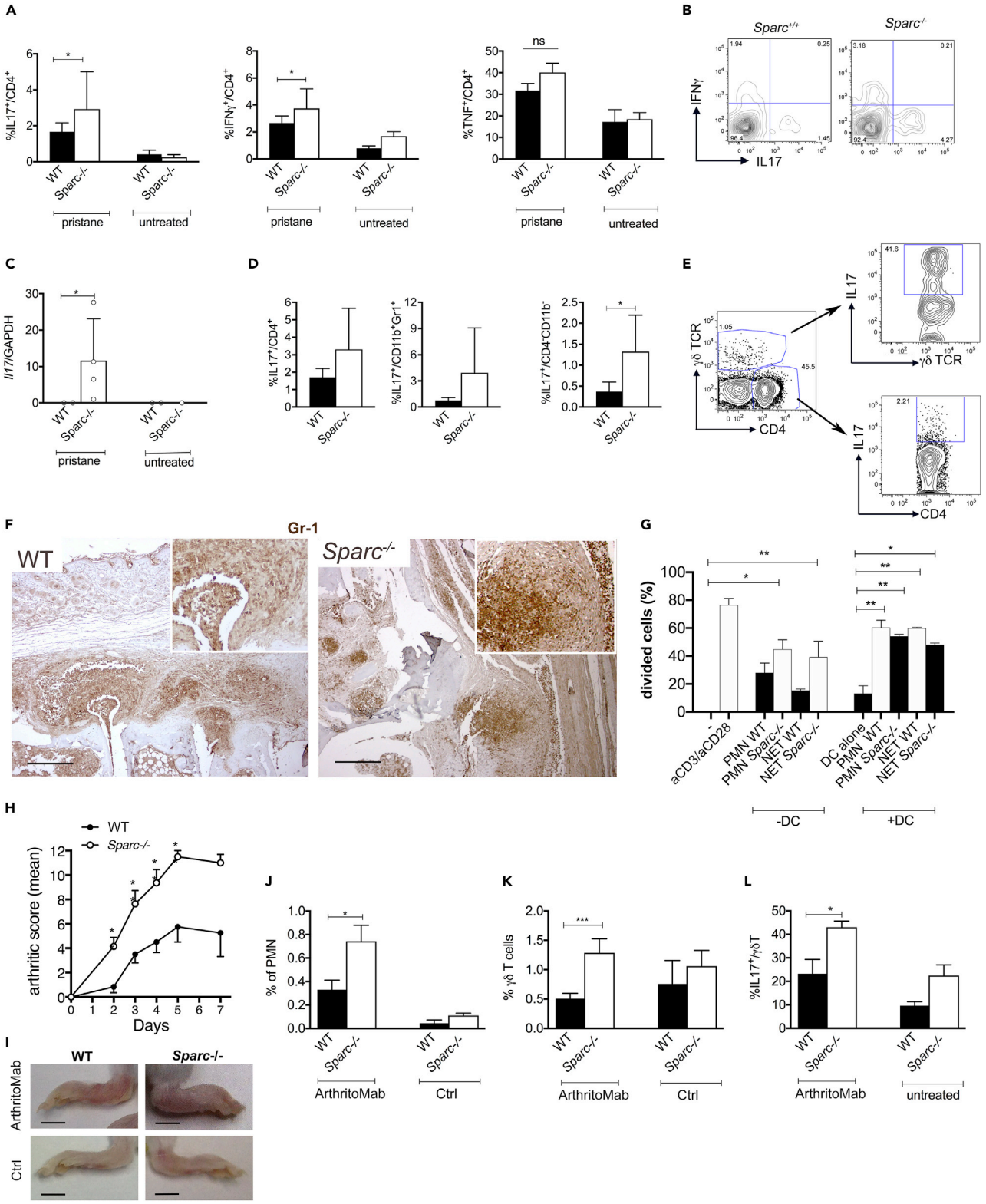

Figure 5. Increased IL-17 production in arthritic paws from Sparc$^{-/-}$ mice

(A–L) (A) Intracellular staining for IL-17, IFNγ, and TNF in CD4^{+} T cells from draining LN of naive and pristane-treated mice (130 days after treatment). Results are representative of three independent experiments (*$p < 0.05$, Student's t test; error bars are mean ± SD). (B) Representative dot plots for the intracellular

Figure 5. *Continued*

staining. (C) qPCR for IL-17A performed by digesting the whole paws of the indicated mice; results are normalized to GAPDH; representative of two other independent experiments; (*p < 0.05, Student's t test; error bars are mean ± SD). (D) Intracellular staining for IL-17 in Th cells ($CD45^+CD4^+$), PMN ($CD45^+CD11b^+Gr1^{hi}$), and other infiltrating cells ($CD45^+CD11b^-CD4^-$) of paws isolated and digested from mice 130 days after pristane injection. (*p < 0.05, Student's t test; error bars are mean ± SD). (E) Production of IL-17 by γδTCR and CD4 cells. Representative plots. (F) IHC analysis for Gr-1 performed on paws obtained from WT and $Sparc^{-/-}$ mice. Scale bar, 500 μm. (G) Frequency of proliferating γδT cells when co-cultured with DC and PMN either from WT or $Sparc^{-/-}$ mice. This analysis highlights a direct capacity of $Sparc^{-/-}$ PMN (either naive or undergoing NETosis) of stimulating γδT cells, independent of the presence of DCs (*p < 0.05; **p < 0.01, Student's t test, mean ± SEM). (H) Arthritis score obtained evaluating arthritis-inducing antibody cocktail (ArthritoMab)-treated mice every 2 weeks (n = 17 mice/group pooled from two independent experiments, *p< 0.05) (I) Representative pictures of paws from WT and $Sparc^{-/-}$ at day 200 treated with ArthritoMab. (J) Frequency of PMN (mean ± SEM), (K) γδT cells (mean ± SEM), and (L) IL-17+ γδT cells (mean ± SEM) in mice treated with ArthritoMab (*p < 0.05; ***p < 0.001; Student's t test).

engulfed by macrophages but not from DCs. On the contrary, when the three populations were from $Sparc^{-/-}$ mice, a relevant number of residual non-phagocytosed PMN was observed, and a notable fraction of PNM materials was uploaded into DCs (Figures 4H and 4I).

This experiment underlined that the pro-inflammatory phenotype of $Sparc^{-/-}$ macrophages combined with a defective clearance of dying PMN could concur to the shift from a tolerogenic to an immunogenic environment licensing DC presentation.

Accumulation and presentation of PMN-derived antigens contribute to the arthritic phenotype

Arthritis is the most relevant phenotype occurring in pristane-treated $Sparc^{-/-}$ mice. Considering the prototypical proinflammatory cytokines IL-17, IFNγ, and TNF involved in the pathogenesis of arthritis, we evaluated their production in pristane-treated WT and $Sparc^{-/-}$ popliteal LN draining paws at day 130, a time point preceding overt tissue damage. We found increased IL-17 and IFNγ in $Sparc^{-/-}$ LN, whereas TNF, although increasing, did not reach statistically significant difference with the WT counterpart (Figures 5A and 5B). In the inflamed joints, the expression of *Il17f* transcript was higher in $Sparc^{-/-}$ than WT mice (Figure 5C). The source of IL-17 was identified in T cells (CD4+), PMN (CD11b + Gr-1+), and γδT cells (CD11b- CD4- γδTCR+) (Figure 5D), with the third population contributing substantially. Indeed, although the frequency of γδT cells was relatively low (between 0.5% and 3%), they were the most potent producers of IL-17 (Figure 5E). The increased granulocytic infiltration (GR-1+ elements) observed histologically in $Sparc^{-/-}$ paws (Figure 5F) were consistent with an IL-17-skewed inflammatory environment and suggested evaluating whether PMN could represent a stimulus for γδT cells either directly or through APCs. To address this point, we set up co-culture experiments in which CFSE-labeled γδT cells were cultured with DCs and PMN from WT or $Sparc^{-/-}$ mice. We found that the concomitant presence of DCs and PMN was required for effective stimulation of γδT cell proliferation in WT conditions. However, when PMN were from $Sparc^{-/-}$ mice they showed a direct capacity of stimulating γδT cell proliferation, efficiently and independently of the presence of DCs (Figure 5G).

These data would suggest that the more severe arthritis observed in $Sparc^{-/-}$ than WT mice, other than the result from accelerated onset of SLE-like autoimmunity, can be exacerbated by the local accumulation of PMN and their stimulation of IL-17-producing γδT cells. To further challenge this hypothesis, we induced arthritis in WT and $Sparc^{-/-}$ mice adopting a mAb-induced arthritis model, a system that uses a pool of four anti-collagen II mAbs (arthritoMab), bypassing, *de facto*, the contribution of systemic SLE-like autoimmunity to generate arthritis. In the mAb-induced model, $Sparc^{-/-}$ mice developed arthritis more rapidly than their WT counterparts (Figures 5H and 5I) and showed popliteal LN enlargement (not shown) and γδT cell enrichment (Figures 5J and 5K) with significant increased production of IL-17 (Figure 5L) and PMN accumulation. Commonalities in PMN recruitment in both autoimmune arthritis models could be explained by the increased complement deposition that can be observed in *Sparc−/−* tissues in the presence of autoimmunity and that has been shown to play a relevant role in PMN recruitment (Pagano et al., 2009). Indeed, immunohistochemical (IHC) analysis for C1q and C3 deposition revealed higher complement deposition in $Sparc^{-/-}$ than WT mice treated with either pristane or arthritoMab cocktail (Figure S3).

Finally, as pristane-induced arthritis in mice surrogate human SLE-associated arthritis we tested the consistency of SPARC expression in humans evaluating published gene expression profiles (Database: GSE36700 [Toukap et al., 2007]) of synovial biopsies of knees affected by Rheumatoid Arthritis, Osteoarthritis, Seronegative Arthritis, and SLE-associated Arthritis. ANOVA test was performed to compare each class of disease, and SPARC had a p value <0.05 showing an overall change of expression with lower expression in patients with SLE who showed an opposite trend for EPSTI1 and MX1 as representative key genes in

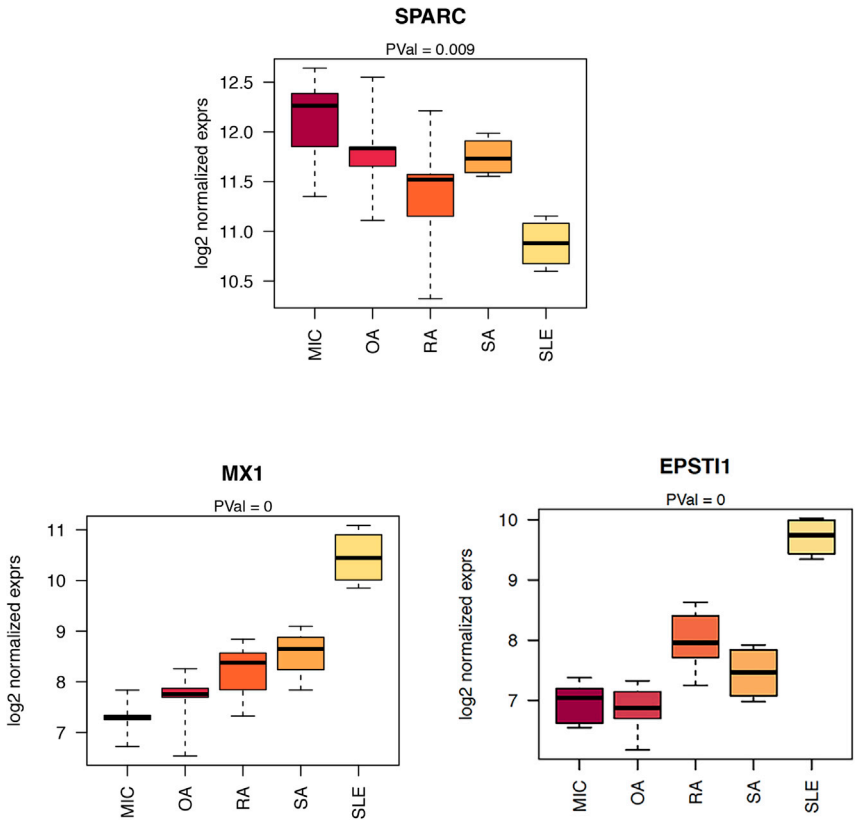

Figure 6. Gene profile analysis of synovial biopsies of knees affected by SLE-associated arthritis
Expression of SPARC, MX1, and EPSTI1 in each class of disease compared with ANOVA test (significance with p value < 0.05).

autoimmunity (Figure 6). This result underscores the possible contribution of SPARC down-regulation in the pathogenesis of SLE and arthritis.

DISCUSSION

This study suggests that *Sparc* down-modulation is a necessary step leading to autoimmunity and RA.

SPARC mediates the correct removal of dying PMN, which otherwise provide a source of nuclear and cytoplasmic autoantigens for the development of autoimmunity. Furthermore, we correlated the inefficient removal of dying cells with RA development (but not ascites) and IL-6 serum level. Indeed, experiments conducted in heterozygous mice clearly show a *Sparc* gene-dosage effect, over neutrophil death, serum IL-6 levels, and the development of RA as these events in heterozygous $Sparc^{+/-}$ mice were at an intermediate level between $Sparc^{-/-}$ and the $Sparc^{+/+}$ mice.

Using the pristane-induced SLE-like disease (Satoh and Reeves, 1994), we show that $Sparc^{-/-}$ mice had anticipated and exacerbated SLE-associated autoimmune manifestations, despite reduced formation of ascites. This last observation was surprising because ascites has been considered a necessary step for the generation of autoantibodies upon pristane challenge (Satoh and Reeves, 1994). Nevertheless, this event seems unnecessary in $Sparc^{-/-}$ mice, because of more efficient DC migration and antigen presentation and increased formation of tertiary lymphoid organs, in the form of OG, which are instrumental in the pathogenesis of systemic autoimmunity (Nacionales et al., 2006). When compared with the *Sparc*-proficient counterpart, OGs from $Sparc^{-/-}$ mice show a preferential accumulation of PMN associated with the presence of cell debris suggestive of active cell death. Accordingly, the peritoneal wash of pristane-treated $Sparc^{-/-}$ mice showed increased numbers of dying PMN, which represent a candidate source of autoantigens. Although exposed to the same pristane treatment, *Sparc*-proficient PMN mostly die by apoptosis, whereas $Sparc^{-/-}$ PMN also showed increased necrosis and NETosis. It might be possible that SPARC deficiency could modify

the outcome of cell death programs allowing PMN, not yet committed toward apoptosis, to release NETs. In this context, we have previously reported that complement deposition and activation (C1q and C5a) are increased in *Sparc*-deficient mice (Tripodo et al., 2017) and that C5a is both an inhibitor of apoptosis (Fishelson et al., 2001) and an inducer of NETosis in the presence of IFNs (Yousefi et al., 2009). The increased complement deposition takes part in autoimmune RA in both models (pristane and mAb-induced) and could be responsible for the worsened disease occurring in Sparc−/− mice also explaining their massive PMN recruitment and stimulation of γδT cells proliferation and IL-17 production.

Another interesting hint comes from the observed robust expression of "don't-eat-me" signals: CD47 and CD31, in $Sparc^{-/-}$ PMN, which could unbalance PMN death toward secondary necrosis and NETosis, in the pristane model. Also in cancer, CD47 overexpression has been associated with decreased PMN apoptosis and phagocytosis (Barrera et al., 2017). Despite the fact that the underlying mechanisms are largely unexplored, *Sparc* deficiency is associated with increased inflammation and secretion of cytokines such as TNF. This is consistent with enhanced activation of the NF-κB pathway as already observed by us in other settings (Sangaletti et al., 2019). Hence, the persistent CD47 and CD31 expression observed here could be explained by the inability of $Sparc^{-/-}$ PMN to inhibit the NF-κB signaling pathway dampening IL-6 production. Indeed, the serum level of IL-6 was higher in $Sparc^{-/-}$ mice and blocking Abs to a-IL6R was inefficient in reducing CD47 and CD31 expression in Sparc−/−, whereas active in WT counterpart.

The increased NETosis of $Sparc^{-/-}$ mice could also account for the higher titer of a-dsDNA autoantibodies. Differently from a-RNP Ab, dsDNA Abs require IL-6 and develop according to the inflammatory peaks of disease (Richards et al., 1998). Although IL-6 is not directly involved in NET formation, the preferential and persistent interaction between NET and DC promotes DC activation and their release of IL-6, toward dsDNA Ab production (Sangaletti et al., 2012). In $Sparc^{-/-}$ mice, the increased NETosis along with the defective macrophages clearance of dying PMN might favor the development of this class of autoantibodies. In support of the DC centrality in this process, we show that DCs, but not macrophages, migrate to draining LNs upon pristane treatment. *In vitro*, co-culture of PMN, DCs, and macrophages shows that the combination of defective macrophages clearance and increased NETosis, associated with the $Sparc^{-/-}$ genotype, allows a more efficient upload of DC with NET components. The clearance of NET and the associated MPO involves the macrophage scavenger receptor CD206/MRC1 (Shepherd and Hoidal, 1990) (Gordon and Pluddemann, 2018). GEP analysis shows that *Sparc*-deficient macrophages express significantly less Mrc1/CD206 than the proficient counterpart. This is partially explained by the preferential M1 polarization of *Sparc*-null macrophage, CD206 expression being almost entirely restricted to M2 macrophages. Such polarization is also supported by the increased expression of genes related to cholesterol homeostasis, which characterize the M1 phenotype. Conversely, M2 macrophages are more dependent on oxidative phosphorylation (OXPHOS) over glycolysis for ATP supply (Oren et al., 1963). Overall, the *Sparc*-deficient condition favors DC uptake of NET debris and their presentation toward a-dsDNA Abs development.

Although we demonstrated that *Sparc* deficiency in mice recapitulates key features of neutrophil defects characterizing patients with SLE (Kaplan, 2011), humans are genetically *Sparc*-proficient. Nevertheless, the persistent presence of IFNs characterizing the initial phase of SLE might create the conditions promoting local SPARC down-modulation. Notably, we have previously shown *Sparc* down-modulation in mice in which peripheral autoimmune conditions were induced (Tripodo et al., 2017). Also, the BM of these mice was characterized by local IFNγ production and down-modulation of Sparc and collagen genes in mesenchymal cells (Tripodo et al., 2017).

Notably, a variety of anti-ds-DNA Ab from patients with SLE target ubiquitary mesenchymal/ECM antigens including a 44-amino-acid fragment of Hevin, a protein belonging to the osteonectin/BM-40/SPARC family. Our link between defective *Sparc* expression and autoimmunity opens new prospects on investigating whether a-ds-DNA Ab targeting SPARC might be part of the pathogenic events leading to autoimmunity and interfering with PMN homeostasis, the latter inspired by the reported capacity of autoantibodies, from SLE sera, to impair PMN functions (Tsai et al., 2019).

Limitations of the study

Our study lacks a formal identification of whether tissue- or leukocytes-derived SPARC is responsible for the reduced clearance of dying neutrophils as trigger of autoimmunity and RA development. We performed bone marrow transplantation experiments in order to dissect the relevant source of SPARC,

but the approached was unfeasible because of the detrimental effect of combining BM transplantation with pristane treatment. Nevertheless, our experiments with Sparc$^{+/-}$ heterozygous mice as well as the gene expression profile analysis of pristane-treated susceptible BALB/c versus non-susceptible DBA/2 mice showed higher expression of *Sparc* in the susceptible strain and its prompt down-modulated after pristane treatment. These data support a gene dosage-dependent effect of SPARC and indicate SPARC down-modulation necessary to license autoimmunity, a finding in line with human GEP of synovial biopsies. In the complexity of autoimmunity pathogenesis, SPARC might play additional role other than our described neutrophils clearance and related events.

STAR★METHODS

Detailed methods are provided in the online version of this paper and include the following:

- KEY RESOURCES TABLE
- RESOURCE AVAILABILITY
  - Lead contact
  - Material availability
  - Data and code availability
- EXPERIMENTAL MODELS AND SUBJECT DETAILS
  - *In vivo* animal studies
- METHOD DETAILS
  - Immunohistochemistry and histopathology
  - Cell preparations
  - *In vivo* blockade of the IL-6 receptor
  - Elisa assay
  - Flow cytometry
  - PMN activation and ROS measurement
  - *In vivo* phagocytosis assay
  - Generation of dendritic cells from BM precursors
  - Macrophages-DC-PMN culture for live cell imaging experiments
  - RNA extraction and semi-quantitative PCR analysis
  - Gene expression profiling analysis
- QUANTIFICATION AND STATISTICAL ANALYSIS

SUPPLEMENTAL INFORMATION

Supplemental information can be found online at https://doi.org/10.1016/j.isci.2021.102510.

ACKNOWLEDGMENTS

This work was supported the Italian Ministry of Health, Italy (Young Researcher Grant number GR-2013-02355637). The authors also thank Mrs. E. Grande for administrative support.

AUTHOR CONTRIBUTIONS

S.S. and M.P.C. conceived and supervised the study, designed experiments, and wrote and approved the manuscript; S.S. analyzed the data and performed the confocal microcopy analysis; D.L., B.B., and P.P. performed *in vitro* experiments and *ex vivo* analysis; A.G., V.C., and C.T. performed IHC and histopathological analysis, L.D.C generated the gene expression data; M.M. and M.D. designed and performed bioinformatic analyses.

DECLARATION OF INTEREST

The authors have no conflict of interest to declare.

Received: August 17, 2020
Revised: December 15, 2020
Accepted: April 30, 2021
Published: June 25, 2021

REFERENCES

Bagavant, H., and Fu, S.M. (2005). New insights from murine lupus: disassociation of autoimmunity and end organ damage and the role of T cells. Curr. Opin. Rheumatol. *17*, 523–528.

Banchereau, J., and Pascual, V. (2006). Type I interferon in systemic lupus erythematosus and other autoimmune diseases. Immunity *25*, 383–392.

Barrera, L., Montes-Servin, E., Hernandez-Martinez, J.M., Garcia-Vicente, M.L.A., Montes-Servin, E., Herrera-Martinez, M., Crispin, J.C., Borbolla-Escoboza, J.R., and Arrieta, O. (2017). CD47 overexpression is associated with decreased neutrophil apoptosis/phagocytosis and poor prognosis in non-small-cell lung cancer patients. Br. J. Cancer *117*, 385–397.

Baumann, I., Kolowos, W., Voll, R.E., Manger, B., Gaipl, U., Neuhuber, W.L., Kirchner, T., Kalden, J.R., and Herrmann, M. (2002). Impaired uptake of apoptotic cells into tingible body macrophages in germinal centers of patients with systemic lupus erythematosus. Arthritis Rheum. *46*, 191–201.

Betancur, P.A., Abraham, B.J., Yiu, Y.Y., Willingham, S.B., Khameneh, F., Zarnegar, M., Kuo, A.H., McKenna, K., Kojima, Y., Leeper, N.J., et al. (2017). A CD47-associated super-enhancer links pro-inflammatory signalling to CD47 upregulation in breast cancer. Nat. Commun. *8*, 14802.

Bratton, D.L., and Henson, P.M. (2011). Neutrophil clearance: when the party is over, clean-up begins. Trends Immunol. *32*, 350–357.

Brekken, R.A., and Sage, E.H. (2001). SPARC, a matricellular protein: at the crossroads of cell-matrix communication. Matrix Biol. *19*, 816–827.

Cairns, A.P., Crockard, A.D., McConnell, J.R., Courtney, P.A., and Bell, A.L. (2001). Reduced expression of CD44 on monocytes and neutrophils in systemic lupus erythematosus: relations with apoptotic neutrophils and disease activity. Ann. Rheum. Dis. *60*, 950–955.

Costenbader, K.H., and Karlson, E.W. (2006). Cigarette smoking and autoimmune disease: what can we learn from epidemiology? Lupus *15*, 737–745.

Davies, K.A., Robson, M.G., Peters, A.M., Norsworthy, P., Nash, J.T., and Walport, M.J. (2002). Defective Fc-dependent processing of immune complexes in patients with systemic lupus erythematosus. Arthritis Rheum. *46*, 1028–1038.

Delany, A.M., Amling, M., Priemel, M., Howe, C., Baron, R., and Canalis, E. (2000). Osteopenia and decreased bone formation in osteonectin-deficient mice. J. Clin. Invest. *105*, 915–923.

Diskin, C., and Palsson-McDermott, E.M. (2018). Metabolic Modulation in Macrophage effector Function. Frontiers in Immunology *9*, 1–17.

Dorner, T., and Furie, R. (2019). Novel paradigms in systemic lupus erythematosus. Lancet *393*, 2344–2358.

Fishelson, Z., Attali, G., and Mevorach, D. (2001). Complement and apoptosis. Mol. Immunol. *38*, 207–219.

Garcia-Romo, G.S., Caielli, S., Vega, B., Connolly, J., Allantaz, F., Xu, Z., Punaro, M., Baisch, J., Guiducci, C., Coffman, R.L., et al. (2011). Netting neutrophils are major inducers of type I IFN production in pediatric systemic lupus erythematosus. Sci. Transl Med. *3*, 73ra20.

Gestermann, N., Di Domizio, J., Lande, R., Demaria, O., Frasca, L., Feldmeyer, L., Di Lucca, J., and Gilliet, M. (2018). Netting neutrophils activate autoreactive B cells in lupus. J. Immunol. *200*, 3364–3371.

Ghosn, E.E., Cassado, A.A., Govoni, G.R., Fukuhara, T., Yang, Y., Monack, D.M., Bortoluci, K.R., Almeida, S.R., Herzenberg, L.A., and Herzenberg, L.A. (2010). Two physically, functionally, and developmentally distinct peritoneal macrophage subsets. Proc. Natl. Acad. Sci. U S A. *107*, 2568–2573.

Gordon, S., and Pluddemann, A. (2018). Macrophage clearance of apoptotic cells: a critical assessment. Front. Immunol. *9*, 127.

Hart, S.P., Ross, J.A., Ross, K., Haslett, C., and Dransfield, I. (2000). Molecular characterization of the surface of apoptotic neutrophils: implications for functional downregulation and recognition by phagocytes. Cell Death Differ *7*, 493–503.

Heeringa, P., Rutgers, A., and Kallenberg, C.G.M. (2018). The net effect of ANCA on neutrophil extracellular trap formation. Kidney Int. *94*, 14–16.

Kaplan, M.J. (2011). Neutrophils in the pathogenesis and manifestations of SLE. Nat. Rev. Rheumatol. *7*, 691–699.

Kessenbrock, K., Krumbholz, M., Schonermarck, U., Back, W., Gross, W.L., Werb, Z., Grone, H.J., Brinkmann, V., and Jenne, D.E. (2009). Netting neutrophils in autoimmune small-vessel vasculitis. Nat. Med. *15*, 623–625.

Lande, R., Ganguly, D., Facchinetti, V., Frasca, L., Conrad, C., Gregorio, J., Meller, S., Chamilos, G., Sebasigari, R., Riccieri, V., et al. (2011). Neutrophils activate plasmacytoid dendritic cells by releasing self-DNA-peptide complexes in systemic lupus erythematosus. Sci. Transl Med. *3*, 73ra19.

Langfelder, P., and Horvath, S. (2008). WGCNA: an R package for weighted correlation network analysis. Bmc Bioinformatics *9*, 559.

Luo, Z., Zhou, Y., Luo, P., Zhao, Q., Xiao, N., Yu, Y., Yan, Q., Lu, G., and Cheng, L. (2014). SPARC deficiency affects bone marrow stromal function, resulting in impaired B lymphopoiesis. J. Leukoc. Biol. *96*, 73–82.

Munoz, L.E., Lauber, K., Schiller, M., Manfredi, A.A., and Herrmann, M. (2010). The role of defective clearance of apoptotic cells in systemic autoimmunity. Nat. Rev. Rheumatol. *6*, 280–289.

Nacionales, D.C., Kelly, K.M., Lee, P.Y., Zhuang, H., Li, Y., Weinstein, J.S., Sobel, E., Kuroda, Y., Akaogi, J., Satoh, M., et al. (2006). Type I interferon production by tertiary lymphoid tissue developing in response to 2,6,10,14-tetramethylpentadecane (pristane). Am. J. Pathol. *168*, 1227–1240.

Norose, K., Clark, J.I., Syed, N.A., Basu, A., Heber-Katz, E., Sage, E.H., and Howe, C.C. (1998). SPARC deficiency leads to early-onset cataractogenesis. Invest. Ophth Vis. Sci. *39*, 2674–2680.

Oren, R., Farnham, A.E., Saito, K., Milofsky, E., and Karnovsky, M.L. (1963). Metabolic patterns in three types of phagocytizing cells. J. Cell Biol *17*, 487–501.

Pagano, M.B., Zhou, H.F., Ennis, T.L., Wu, X.B., Lambris, J.D., Atkinson, J.P., Thompson, R.W., Hourcade, D.E., and Pham, C.T.N. (2009). Complement-dependent neutrophil recruitment is critical for the development of elastase-induced abdominal aortic aneurysm. Circulation *119*, 1805–U1197.

Piconese, S., Costanza, M., Tripodo, C., Sangaletti, S., Musio, S., Pittoni, P., Poliani, P.L., Burocchi, A., Passafaro, A.L., Gorzanelli, A., et al. (2011). The matricellular protein SPARC supports follicular dendritic cell networking toward Th17 responses. J. Autoimmun. *37*, 300–310.

Puolakkainen, P., Bradshaw, A.D., Kyriakides, T.R., Reed, M., Brekken, R., Wight, T., Bornstein, P., Ratner, B., and Sage, E.H. (2003). Compromised production of extracellular matrix in mice lacking secreted protein, acidic and rich in cysteine (SPARC) leads to a reduced foreign body reaction to implanted biomaterials. Am. J. Pathol. *162*, 627–635.

Ravichandran, K.S. (2011). Beginnings of a good apoptotic meal: the find-me and eat-me signaling pathways. Immunity *35*, 445–455.

Reeves, W.H., Lee, P.Y., Weinstein, J.S., Satoh, M., and Lu, L. (2009). Induction of autoimmunity by pristane and other naturally occurring hydrocarbons. Trends Immunol. *30*, 455–464.

Rekvig, O.P., and Nossent, J.C. (2003). Anti-double-stranded DNA antibodies, nucleosomes, and systemic lupus erythematosus: a time for new paradigms? Arthritis Rheum. *48*, 300–312.

Richards, H.B., Satoh, M., Shaw, M., Libert, C., Poli, V., and Reeves, W.H. (1998). Interleukin 6 dependence of anti-DNA antibody production: evidence for two pathways of autoantibody formation in pristane-induced lupus. J. Exp. Med. *188*, 985–990.

Rosenblum, M.D., Remedios, K.A., and Abbas, A.K. (2015). Mechanisms of human autoimmunity. J. Clin. Invest. *125*, 2228–2233.

Sangaletti, S., Talarico, G., Chiodoni, C., Cappetti, B., Botti, L., Portararo, P., Gulino, A., Consonni, F.M., Sica, A., Randon, G., et al. (2019). SPARC is a new myeloid-derived suppressor cell marker licensing suppressive activities. Front. Immunol. *10*, 1369.

Sangaletti, S., Tripodo, C., Cappetti, B., Casalini, P., Chiodoni, C., Piconese, S., Santangelo, A., Parenza, M., Arioli, I., Miotti, S., et al. (2011). SPARC oppositely regulates inflammation and fibrosis in bleomycin-induced lung damage. Am. J. Pathol. *179*, 3000–3010.

Sangaletti, S., Tripodo, C., Chiodoni, C., Guarnotta, C., Cappetti, B., Casalini, P., Piconese, S., Parenza, M., Guiducci, C., Vitali, C., et al. (2012). Neutrophil extracellular traps mediate transfer of cytoplasmic neutrophil antigens to myeloid dendritic cells toward ANCA induction and associated autoimmunity. Blood *120*, 3007–3018.

Sangaletti, S., Tripodo, C., Portararo, P., Dugo, M., Vitali, C., Botti, L., Guarnotta, C., Cappetti, B., Gulino, A., Torselli, I., et al. (2014a). Stromal niche communalities underscore the contribution of the matricellular protein SPARC to B-cell development and lymphoid malignancies. Oncoimmunology *3*, e28989.

Sangaletti, S., Tripodo, C., Vitali, C., Portararo, P., Guarnotta, C., Casalini, P., Cappetti, B., Miotti, S., Pinciroli, P., Fuligni, F., et al. (2014b). Defective stromal remodeling and neutrophil extracellular traps in lymphoid tissues favor the transition from autoimmunity to lymphoma. Cancer Discov. *4*, 110–129.

Satoh, M., and Reeves, W.H. (1994). Induction of lupus-associated autoantibodies in BALB/c mice by intraperitoneal injection of pristane. J. Exp. Med. *180*, 2341–2346.

Shepherd, V.L., and Hoidal, J.R. (1990). Clearance of neutrophil-derived myeloperoxidase by the macrophage mannose receptor. Am. J. Respir. Cell Mol Biol *2*, 335–340.

Toukap, A.N., Galant, C., Theate, I., Maudoux, A.L., Lories, R.J.U., Houssiau, F.A., and Lauwerys, B.R. (2007). Identification of distinct gene expression profiles in the synovium of patients with systemic lupus erythematosus. Arthritis Rheum-Us *56*, 1579–1588.

Tripodo, C., Burocchi, A., Piccaluga, P.P., Chiodoni, C., Portararo, P., Cappetti, B., Botti, L., Gulino, A., Isidori, A., Liso, A., et al. (2017). Persistent immune stimulation exacerbates genetically driven myeloproliferative disorders via stromal remodeling. Cancer Res. *77*, 3685–3699.

Tripodo, C., Sangaletti, S., Guarnotta, C., Piccaluga, P.P., Cacciatore, M., Giuliano, M., Franco, G., Chiodoni, C., Sciandra, M., Miotti, S., et al. (2012). Stromal SPARC contributes to the detrimental fibrotic changes associated with myeloproliferation whereas its deficiency favors myeloid cell expansion. Blood *120*, 3541–3554.

Trombetta-Esilva, J., and Bradshaw, A.D. (2012). The function of SPARC as a mediator of fibrosis. Open Rheumatol. J. *6*, 146–155.

Tsai, C.Y., Li, K.J., Hsieh, S.C., Liao, H.T., and Yu, C.L. (2019). What's wrong with neutrophils in lupus? Clin. Exp. Rheumatol. *37*, 684–693.

Yousefi, S., Mihalache, C., Kozlowski, E., Schmid, I., and Simon, H.U. (2009). Viable neutrophils release mitochondrial DNA to form neutrophil extracellular traps. Cell Death Differ *16*, 1438–1444.

Zhang, K., Kagan, D., DuBois, W., Robinson, R., Bliskovsky, V., Vass, W.C., Zhang, S.L., and Mock, B.A. (2009). Mndal, a new interferon-inducible family member, is highly polymorphic, suppresses cell growth, and may modify plasmacytoma susceptibility. Blood *114*, 2952–2960.

STAR★METHODS

KEY RESOURCES TABLE

REAGENT or RESOURCE	SOURCE	IDENTIFIER
Antibodies		
Name	Company	Clone/Cat. number
MFG-E8	R&D	340614/cat#MAB-2805; RRID: AB_2297564
C3	Abcam	11H9/cat#ab11862; RRID: AB_2066623
GR-1	eBioscience	RB6-8C5/cat#53-5931-82; RRID: AB_469918
F4/80	Biolegend	BM8.1/cat#123114; RRID: AB_893478
CD11b	TONBO Biosc.	M1/70/cat#50-0112-U100; RRID: AB_11218507
CD4	eBioscience	RM4-5/cat#47-0047-42; RRID: AB10804505
CD11c	eBioscience	N418/cat#17-0114-82; RRID: AB_469346
CD44	BD	IM7/cat#560570; RRID: AB_1727486
CD62L	BD	MEL-14/cat#560516 RRID: AB_1645257
CD69	eBioscience	H1.2F3/cat#11-0691-85; RRID: AB_465120
gdTCR	eBioscience	eBioGL3/cat#12-9959-42; RRID: AB_1603300
Calreticulin	abcam	FMC75/cat#ab83220; RRID: AB_1859755
CD47	eBioscience	Miap301/cat#17-0471-82; RRID: AB_1724083
CD31	eBioscience	MEC13.3/cat#11-0311-85; RRID: AB_465013
IL-6	BD	MP5-20F3/cat#554401; RRID: AB_395367
IFNg	eBioscience	XMG1.2/cat#45-7311-82; RRID: AB_1107020
IL-17	BD	eBio17B7/cat#564170; RRID: AB_2738641
TNF	Biolegend	MP6-XT22/cat#506313; RRID: AB_493328
IL-4	eBioscience	BVD6-24G2/cat#12-7041-81; RRID: AB_466155
P65	Cell Signaling	L8F6/cat#94605;RRID: AB_10828935
Phospho-P65	Cell Signaling	93H1/cat#3033T; RRID: AB_10706937
IkBa	Cell Signaling	L35A5/cat#5743; RRID: AB_10695750
Phospho-IkBa	Cell Signaling	14D4/cat#2859; RRID: AB_561111
Chemicals, peptides, and recombinant proteins		
Name	Company	Catalog number
2,6,10,14-Tetramethylpentadecane	Sigma-Aldrich	P9622
LPS	Sigma-Aldrich	P9622
rGM-CSF (mouse)	Peprotech	315-03
rIL4 (mouse)	Peprotech	214-14
Critical commercial assays		
anti-dsDNA ELISA Kit	Alpha Diagnostic Int.	5110
nRNP ELISA Kit	Alpha Diagnostic Int.	5410
ANA ELISA KIt	Alpha Diagnostic Int.	5210
ssDNA ELISA KIt	Alpha Diagnostic Int.	5310
RF ELISA Kit	Alpha Diagnostic Int.	6200
Sm ELISA KIt	Alpha Diagnostic Int.	5405
2,6,10,14-Tetramethylpentadecane	Sigma-Aldrich	P9622
Annexin V Apoptosis Detection Kit	eBioscience	88-8005-74

(*Continued on next page*)

Continued

REAGENT or RESOURCE	SOURCE	IDENTIFIER
7-AAD	eBioscience	00-6993-50
PKH26	Sigma-Aldrich	PKH26GL
Wheat Germ Agglutinin, Alexa Fluor™ 633 Conjugate	Invitrogen	W21404
SYTOX™ Green	Invitrogen	S7020
InSolution™ NF-κB Activation Inhibitor	Calbiochem	481407
IL-6 ELISA Kit	Invitrogen	BMS603-2TW0
Dihydrorhodamine 123	Invitrogen	HY-101894
CFSE	Invitrogen	65-0850-84
Deposited data		
Specifications	Repository	Accession number
Gene expression profile of PerC macrophages obtained from WT or *Sparc−/−* mice treated with pristane	NCBI's Gene Expression Omnibus (GEO).	GSE144415
Gene expression from synovial biopsies of 25 patients affected by: Rheumatoid arthritis (RA), seronegative arthritis (SA), systemic lupus erythematosus (SLE) and osteoarthritis (OA).	NCBI's Gene Expression Omnibus (GEO)	GSE36700 https://doi.org/10.1002/art.22578 https://pubmed.ncbi.nlm.nih.gov/17469140/
Gene expression from rom mesentery of pristane treated and control animals	NCBI's Gene Expression Omnibus (GEO)	GSE17297 https://doi.org/10.1182/blood-2009-01-198812 https://pubmed.ncbi.nlm.nih.gov/19654412/
Experimental models: Organisms/strains		
Sparc$^{<tm1Hwe>}$/CNCr *Sparc*$^{-/-}$ mice on a mixed 129SV/C57BL/6 background were originally provided by Prof. C. Howe (The Wistar Institute, Philadelphia, PA). Mice were backcrossed for 12 generations in our animal facility with BALB/cAnNCrl (Charles River Laboratories), to obtain congenic *Sparc*$^{-/-}$ mice.	Laboratory of dr. M.P. Colombo	Proprietary not commercial
Oligonucleotides		
Gene	Company	Code
ActB	TaqMan	Mm02619580_g1
Sparc	TaqMan	Mm00446190_m1
Il17	TaqMan	Mm00439618_m1
Software and algorithms		
Name	Company	Site
Prism *vs.* 8	GraphPad	https://www.graphpad.com/scientific-software/prism/
Lumi package	Bioconductor	https://www.bioconductor.org/packages/release/bioc/html/lumi.html
WCGNA R software package	UCLA	https://horvath.genetics.ucla.edu/html/CoexpressionNetwork/Rpackages/WGCNA/
FlowJo vs.10	FlowJo-BD	https://www.flowjo.com/solutions/flowjo/downloads
Zen 2.0 software	Zeiss	https://www.zeiss.com/microscopy/int/products/microscope-software/zen-lite.html
ImageProPlus *vs* 4.5	Media-Cybernetics	https://www.mediacy.com/imageproplus

RESOURCE AVAILABILITY

Lead contact

Further information and request should be directed to and will be fulfilled by the corresponding author Sabina Sangaletti (sabina.sangaletti@istitutotumori.mi.it)

Material availability

This study did not generate unique reagents. Sparc$^{<tm1Hwe>}$/CNCr mice will be available upon resonable request. Details are in the KRT.

Data and code availability

The dataset GSE144415 generated during this study, GSE36700 and GSE144415 are available at GEO repository at the following addresses: https://www.ncbi.nlm.nih.gov/geo/query/acc.cgi?acc=GSE144415; https://www.ncbi.nlm.nih.gov/geo/query/acc.cgi?acc=GSE36700; https://www.ncbi.nlm.nih.gov/geo/query/acc.cgi?acc=GSE17297.

EXPERIMENTAL MODELS AND SUBJECT DETAILS

In vivo animal studies

Sparc$^{-/-}$ and WT mice were on BALB/c background and were bred and maintained in our animal facility. *Sparc*$^{-/-}$ mice on a mixed 129SV/C57BL/6 background were provided by C. Howe (The Wistar Institute, Philadelphia, PA). Mice were backcrossed for 12 generations with BALB/cAnNCrl (Charles River Laboratories) to obtain congenic *Sparc*$^{-/-}$ mice.

In some experiments WT mice were purchased from Charles River. Experiments were performed according to local ethical guidelines. Authorization number (internal ethical committee): INT_10/2011).

Female of 8-10 week of age were injected intraperitoneally with 0.5 mL of Pristane (2,6,10,14-Tetramethylpentadecane, Sigma-Aldrich) at day 0, 60 and 120 and monitored every two weeks for signs of arthritis. Severity of arthritis was evaluated in a blind fashion for each paw per mouse with a 0–3 score (maximum 12 pt each animal): 0, no arthritis; 1, mild joint swelling and erythema; 2, severe joint and digit swelling; 3, paw deformation and ankylosis.

For Collagen Antibody Induced Arthritis (CAIA), 2 mg of ArthritoMab Antibody cocktail were administered i.v. on day 0 and 50, LPS was administered i.p. on day 3 (All from MDBiosciences). All four paws were scored daily using a 0–3 score.

METHOD DETAILS

Immunohistochemistry and histopathology

Tissues were dissected from mice, washed in PBS and collected for fixation in 10% neutral buffered formalin and included in paraffin.

Bone samples were decalcified for 8 hr using an EDTA-based decalcifying solution (MicroDec EDTA-based, Diapath), washed out with water for 1 hr and subsequently processed and embedded in paraffin.

Four-micrometers-thick sections were used for both histopathology and immunostaining. Immunohistochemistry was performed using the horseradish peroxidase (HRP) method.

Briefly, tissue samples were deparaffinized, rehydrated and unmasked in Epitope Retrieval Solutions pH9 (Novocastra UK) at 98°C for 30 min in a thermostatic bath.

Subsequently, the sections were brought to room temperature and washed in PBS. After neutralization of the endogenous peroxidase with 3% H_2O_2 and Fc blocking by a specific protein block (Novocastra UK), the samples were incubated over night with primary antibodies: rabbit anti-mouse C1q 1:400, kindly provided by F. Tedesco, University of Trieste and rabbit anti-mouse C3 1:200 (Sigma Aldrich). The staining was revealed using donkey anti-rabbit IgG (H&L) specific secondary antibody 1:500 (Novex by Life Technologies)

and AEC (3-Amino-9-ethylcarbazole) substrate-chromogen. The slides were counterstained with Harris hematoxylin (BioCare).

Slides were analyzed under an Axioscope A1 microscope equipped with an Axiocam 503 Color digital camera and Zen 2.0 Software (Zeiss).

Histological tissue damage in kidney, lung and liver samples was evaluated on H&E-stained sections. For the determination of the damage score, the tissue involvement was scored as 1 (less than 25% involvement), 2 (25% to less than 50% involvement) or 3 (50% or greater involvement) for each of the following variables: glomerular cellularity, glomerular necrosis, glomerular sclerosis, presence of glomerular crescents, interstitial inflammatory infiltrate, interstitial fibrosis.

In the liver, the severity of parenchymal damage was scored as mild 1, moderate 2 or severe 3.

For the lung tissue damage score, the presence of plasmacytoma infiltration was scores as partial infiltration, 1 or diffuse infiltration, 2. The alveolar septa thickening, interstitial inflammatory infiltrate, fibroblastic proliferation, epithelial proliferation and pulmonary parenchymal damage were scored as focal 1, multifocal 2 or diffuse 3.

Cell preparations

Peritoneal lavage was performed by infusing 10 mL of sterile PBS. Peritoneal PMN and macrophages were separated seeding peritoneal cells for 30 min, this allow macrophages to adhere to the cell culture plate. PMN, which remain in the floating fraction, can be harvested by gently washing the plate. PMN and macrophages purity was up to 90%.

The evaluate the impact of NF-kB over neutrophil death and expression of don't eat me signals, PMN isolated from pristane-treated mice were treated with the NF-kB inhibitor (InSolution NF-kBinhibitor, Calbiochem, 10 nM) during the o/n culture (peritoneal neutrophils from day 130).

To prove the role of SPARC in controlling NF-kB signaling we performed a canonical assay in which PMN isolated from peritoneal wash were stimulated with LPS (100 ng/mL, Sigma-Aldrich) for 2h and then evaluated for the phosphorilation of p65 and IkBa by FACS analysis (see Table below).

Hind paws cell suspension were obtained chopping paws into small pieces. Pieces were resuspended in HBSS and digested in 1mg/ml collagenase IV (Sigma-Aldrich) at 37°C for 1 hr; digested tissue were passed through 70 μm cell strainer and cell suspension were used for subsequent analysis.

In vivo blockade of the IL-6 receptor

For IL6R blockade mice were administrated with pristane and treated with the 15A7 blocking Ab (200 μg) for two weeks every two days. The expression of eat-me and don't-me signals was evaluated on peritoneal wash isolated PMN and after the o/n culture.

Elisa assay

To detect autoantibodies in the serum of pristane-treated mice, we used different ELISA kits. Quantitative determination of autoantibodies to dsDNA, ssDNA, ANA, RNP, RF, Sm was performed using kits from Alpha Diagnostic.

Flow cytometry

Surface staining was performed on single cell suspension using the fluorochrome-conjugated monoclonal antibodies to CD11b, F4/80, Gr-1, CD4, CD11c, CD44, CD62L, CD69, γδTCR, CD47, CD31.

AnnexinV/7AAD staining was performed using products and instructions from eBioscience. For intracellular staining of lymphocytes, cells were first stimulated 4 hr *in vitro* with Cell Stimulation Cocktail (plus protein transport inhibitors) (eBioscience). Then cells were surface stained as above and fixed 20 min using the IC fixation buffer, followed by incubation with monoclonal antibodies against IL-17, IL-4, TNF, IFNγ, and resuspendend in Permeabilization Buffer (all from eBioscience). Samples were acquired on the LSR II

(BD Biosciences) and analyses were performed using FlowJo software (BD). To detect IL-6 in myeloid cells we used the same kit but without using the Cell Stimulation Cocktail.

PMN activation and ROS measurement

Peritoneal cavity (PerC) cells of WT and *Sparc*$^{-/-}$ were seeded in 96 well plates and incubated 5 min at 37°C with Dihydrorhodamine 123 (DHR 123) 5 μg/mL in medium, washed and incubated with APC conjugated anti mouse Gr1 for 15'. After washing, cells were activated using phorbol-12-myristate-13-acetate (PMA) 100 ng/mL for the indicated time, after which activation was blocked immediately by diluting samples with fresh medium and keeping cells in ice. Samples were acquired immediately using BD LSR Fortessa; PMN were identified using physical parameters and Gr1 expression and mean fluorescence intensity (MFI) of Rhodamine123 positive cells was calculated.

In vivo phagocytosis assay

To evaluate phagocytosis activity of PerC macrophages, WT or *Sparc*$^{-/-}$ mice were treated with 1 mL thioglycollate i.p. 4 days later, CFSE (65-0850-84 Invitrogen) labeled Jurkat cells were RX irradiated for 8 min (RAD_SOURCE_RS-2000 15 Gy) to induce apoptosis and injected in the PerC of treated mice. After 30 min, PerC were washed and the frequency of macrophages that have engulfed CFSE + apoptotic bodies were examined and indicated as % of phagocytizing F4/80^{high} and F4/80 ^{int} macrophages. CFSE labeling of Jurkat cells was performed adding 5 nM concentration of CFSE to 1 × 10^{6}/mL of cells in RPMI without serum for 20 min at 37°C. Cells were then washed two times in complete medium.

Generation of dendritic cells from BM precursors

Bone marrow cells were resuspended at 2 × 10^{6} cells/mL in RPMI 1640 supplemented with 5 ng/mL of rGM-CSF and 10 ng/mL of murine rIL-4 (Peprotech). Half of the medium was replaced with fresh medium containing GM-CSF and IL-4 at day 3 and day 5. On day 8-10, loosely adherent cells were harvested by gentle pipetting and mDCs were purified with CD11c MiniMacs columns according to the manufacturer's instructions (Miltenyi Biotec). Phenotype of the purified CD11c^{+} fraction was analyzed by flow cytometry using Abs to CD11c and CD11b.

Macrophages-DC-PMN culture for live cell imaging experiments

Macrophages (4 × 10^{5}) were seeded onto poly-D-lysine coated tissue culture dishes (35 mm) specific for immunofluorescence and confocal microscopy (FluoroDish, Word Precision Instruments, Inc), allowed to adhere for 2 hr and then added with PKH-26 labeled PMN (2 × 10^{5}).

For macrophages/PMN/DC culture, PMNs (2 × 10^{5}) were seeded onto FluoroDish poly-D-lysine coated tissue culture dishes (35 mm) and allowed to adhere for 4 hr in the presence of the DNA SYTOXgreen dye (1:5,000, Invitrogen), which stains only the dsDNA of NETotic/apoptotic cells and is excluded from live cells. Cells were then carefully washes and added with macrophages (2 × 10^{5}) and DC (2 × 10^{5}), which were labeled with the vital dye PKH26 or the Wheat Germ Agglutinin (WGA) (Alexa Fluor 633 Conjugate, Invitrogen), respectively. For the WGA staining cells were incubated 10 min in a 5 μg/mL of WGA/HBSS solution. PKH26 labeling of PMN or macrophages was performed using a 20 μM solution of PKH26 (Sigma-Aldrich). Cell interaction in both experiments were observed by live cell imaging performed on a BioRad laser scanner confocal (Microradiance 2000) using a × 20, 0.5 NA Plan-Fluor DIC dry objective. The microscope (NIKON TE300 ECLIPSE) was equipped with incubation chamber, which provided a humidified atmosphere at 37°C with 5% CO_2. Incorporation of apototic PMN or debris by macrophages or mDCs was performed on confocal microscopy micrographs using the software-assisted (ImageProPlus) technique.

RNA extraction and semi-quantitative PCR analysis

Total RNA was isolated using the Quick-RNA Microprep Kit (R1051-ZYMO RESEARCH). 1μg RNA was reverse-transcribed using High Capacity cDNA Reverse Transcription Kit (ThermoFisher Scientific). The resultant cDNA was analyzed by quantitative PCR using TaqMan Fast Universal PCR Master Mix (ThermoFisher Scientific) with TaqMan Gene Expression Assays (ThermoFisher Scientific) using primers. qRT-PCR experiments were performed in triplicate on a QuantStudio3 (Applied Biosystems). Delta Ct values were normalized to *ActB* and raised to the power of −2. Standard deviations refer to technical replicates.

Gene expression profiling analysis

PerC macrophages obtained from WT or *Sparc−/−* mice were extracted using RNAeasy micro kit (Qiagen). After quality check and quantification by 2100 Bioanalyzer system (Agilent) and Nanodrop ND-1000 spectrophotometer (ThermoFisher), respectively, gene expression was assessed using Illumina BeadChip following manufacture's protocol.

Raw expression data were collected from scanned images using Illumina BeadStudio v3.3.8 and processed using the *lumi* package from Bioconductor. Raw data were log_2-transformed, normalized with robust spline normalization and filtered, keeping only probes with a detection p value < 0.01 in at least one sample. Multiple probes mapping to the same gene symbol were collapsed using the collapse Rows function of the WCGNA package with "MaxMean" method. Expression data were deposited in NCBI's Gene Expression Omnibus (GEO) database with accession number GSE144415.

Differentially expressed genes were identified using *limma* package. p values were corrected for multiple testing using the Benjamini-Hochberg false discovery rate (FDR) method. An FDR <0.25 was applied to select differentially expressed genes. Gene Set Enrichment Analysis (GSEA) was performed using the fgsea package and hallmark gene sets collected from the MSigDB database (http://www.broadinstitute.org/gsea/msigdb/index.jsp) by ranking genes according to their t-statistic. Significantly enriched gene sets were selected according to an FDR <0.05.

We selected GSE36700 dataset from NCBI, which contained gene expression of synovial biopsies from a total of 25 patients affected by: Rheumatoid Arthritis (RA), Seronegative Arthritis (SA), Systemic Lupus Erythematosus (SLE) and Osteoarthritis (OA). Those samples were profiled with Affymetrix Human Genome U133 Plus 2.0 microarrays. Normalized data were collected from GEO repository, probes without their corresponding gene symbol were removed and multiple probes associated to the same gene symbol were collapsed using the collapse Rows function of the WCGNA package with "maxRowVariance" method (Langfelder and Horvath, 2008). To discover an overall change of expression in each class of disease a selected list of genes was tested with ANOVA and the variation was considered significant with p Value < 0.05. Significant pairwise differences (p Value < 0.05) were identified using the post-hoc Tukey's honest significance test. Single sample gene set enrichment analysis (ssGSEA) was performed with the GSVA package for two hallmark pathways retrieved from MSigDB database: epithelial mesenchymal transition and interferon gamma response; then t test was computed to find intra-disease gene set variations and comparison was considered significant with the false discovery rate (FDR) < 0.05, calculated with the Benjamini & Hochberg correction.

Afterward, we analyzed GSE17297, a gene expression derived from BALB\c, DBA2 and CDF1 mice treated/untreated with TMPD. Three and eighteen days after treatment, total RNA was extracted from the mesentery of experimental control animals and profiled with Affymetrix Mouse Genome 430 2.0 Array. Pre-processed data were downloaded with getGEO function from the GEOquery package and log2 transformed. Multiple probes associated to the same gene symbol were collapsed using the collapseRows function from the WCGNA package with the "maxRowVariance" method. Class comparison was performed with the limma package and p.value was corrected with the Benjamini & Hochberg method: genes were considered significant with FDR<0.05. Three and eighteen days treated/untreated animals were considered as a single group denoted respectively as treatment or control.

QUANTIFICATION AND STATISTICAL ANALYSIS

All statistical analyses were performed using Prism 8 software (GraphPad Software). The statistics applied to each experiment are shown in the respective figure legends. We applied both parametric and non-parametric analyses, including Student's t-test and Mann-Whitney test, according to data distribution (normality test). For multiple comparisons, we used one-way ANOVA analysis (Tukey). Ascites and arthritis score data were analyzed through a Long-Rank (Mantel-Cox) test. The number of animals used for *in vivo* experiments has been estimated on the basis of statistical principles to assure the significance of the results with the smallest number of animals. Generally, a power of 0.8 was considered, with α error probability of 5%, and an effect size of 0.4.